AAEC/PR42-P
INDC(AUL)-24/G

NOT FOR PUBLICATION
See note overleaf

XA04N2776

AAEC/PR42-P
INDC(AUL)-26/G

INIS-XA-N--164

# AUSTRALIAN ATOMIC ENERGY COMMISSION

## RESEARCH ESTABLISHMENT

## LUCAS HEIGHTS

PROGRESS REPORT OF PHYSICS DIVISION

1st OCTOBER, 1975-30th SEPTEMBER, 1976

ACTING DIVISION CHIEF - MR. W. GEMMELL

NOT FOR PUBLICATION

AUSTRALIAN ATOMIC ENERGY COMMISSION

RESEARCH ESTABLISHMENT

LUCAS HEIGHTS

# PROGRESS REPORT OF PHYSICS DIVISION

1st OCTOBER, 1975-30th SEPTEMBER, 1976

ACTING DIVISION CHIEF - MR. W. GEMMELL

CONTENTS


| | | Page |
|---|---|---|
| 1. | INTRODUCTION | 1 |
| 2. | REACTOR STUDIES | 2 |
| | 2.1 Moata | 2 |
| | 2.1.1 Moata Operations: Uranium Ore Analysis, Neutron Radiograpy, Obsidian | 2 |
| | 2.1.2 Fluorine neutron activation analysis | 3 |
| | 2.1.3 Moata transients | 3 |
| | 2.2 Critical Facility | 5 |
| | 2.2.1 Reactor noise measurements | 6 |
| | 2.3 Pulsed Integral Experiments with Heavy Metal Assemblies | 6 |
| | 2.4 Neutron Spectrometry | 7 |
| | 2.5 Reactor Safety Studies | 10 |
| | 2.5.1 Calculation of SPERT transients - forced coolant flow | 10 |
| | 2.5.2 LOCA analysis | 12 |
| | 2.5.3 Fission product decay energy | 15 |
| | 2.6 HIFAR | 16 |
| | 2.6.1 HIFAR dynamics | 16 |
| | 2.6.2 X-170 rig support | 16 |
| | 2.6.3 Criticality | 16 |
| | 2.7 Deep Ocean Currents and the Disposal of Radioactive Waste | 17 |
| | 2.8 Assistance to Indonesia | 17 |
| | 2.9 Neutron Source Project | 18 |
| 3. | NEUTRON PHYSICS | 19 |
| | 3.1 3 MeV Accelerator: operations, data acquisition facilities | 19 |
| | 3.2 Fission Studies | 21 |
| | 3.2.1 Measurement of $^{252}$Cf fission neutron spectrum | 21 |
| | 3.2.2 Fission fragment angular distributions for $^{232}$Th | 22 |
| | 3.2.3 $\bar{\nu}_p$ measurements for neutron fission of $^{232}$Th | 25 |
| | 3.2.4 Dynamics of fission | 25 |
| | 3.2.5 Even-odd effects in the neutron emission from $^{252}$Cf spontaneous fission fragments | 26 |
| | 3.3 Neutron Capture Physics | 26 |
| | 3.3.1 Resonance neutron capture systematics | 26 |
| | 3.3.2 s-wave level spacings | 29 |
| | 3.3.3 Neutron capture cross sections | 29 |
| | 3.3.4 Total cross sections | 33 |
| | 3.3.5 Partial capture cross sections of $^{91}$Zr, $^{111,113}$Cd, $^{117,119}$Sn | 35 |
| | 3.3.6 Non-statistical effects in neutron capture | 35 |
| | 3.3.7 Neutron flux measurements | 38 |
| | 3.4 Prompt Nuclear Analysis Obsidian, glass, silica gettering, solar absorber surfaces, Ancient bronze, external beam, thorium, fluorine, bibliography | 38 |

CONTENTS (cont'd)


| | Page |
|---|---|
| 4. THEORETICAL PHYSICS | 42 |
| 4.1 AUS Modular Scheme | 42 |
| 4.1.1 AUS module EDIT | 42 |
| 4.1.2 AUS module MIRANDA | 42 |
| 4.1.3 AUS.ENDF/B cross section library | 42 |
| 4.2 Radiation Shielding | 42 |
| 4.2.1 Shielding codes | 42 |
| 4.2.2 Modified diffusion theory for neutron shielding | 43 |
| 4.2.3 Gamma ray spectrum from ores | 44 |
| 4.3 Proton Recoil Liquid Scintillator Neutron Spectrometers | 44 |
| 4.4 Reactor Data | 45 |
| 4.4.1 Fission product cross section library | 45 |
| 4.4.2 Resonance parameter analysis | 45 |
| 4.4.3 Statistical theory | 46 |
| 4.4.4 Reactor calculations and nuclear information | 46 |
| 4.5 New Reactor Study - Potential of Various Reactor Types for isotope Production | 47 |
| 4.6 Other Items | 48 |
| 4.6.1 Inverse reaction problem | 48 |
| 4.6.2 Interactive computer system | 48 |
| 4.6.3 Interactive least squares fitting program | 49 |
| 4.6.4 Applications of unfolding techniques | 50 |
| 4.7 An Australian Energy Data File | 52 |
| 5. RUM JUNGLE ENVIRONMENTAL STUDIES | 53 |
| 6. PUBLICATIONS | 55 |
| 6.1 Papers | 55 |
| 6.2 Reports | 56 |
| 6.3 Conference Papers | 57 |
| | |
| Table 3.1 Accelerator time allocation | 20 |
| Table 3.2 Experimental $\bar{\nu}_p$ values | 25 |
| Table 3.3 Sodium content of glass | 39 |

CONTENTS (cont'd)


| | | Page |
|---|---|---|
| Figure 2.1 | Moata transients: experiments and ZAPP calculations | 4 |
| Figure 2.2 | Moata transients: effect of coolant flow on power burst shape | 4 |
| Figure 2.3 | Neutron energy spectrum from 2.8 MeV proton irradiation of a thick lithium target at $0^{o}$ to the incident beam | 8 |
| Figure 2.4 | Neutron energy spectrum from 1.4 MeV deuteron irradiation of beryllium at $150^{o}$ to incident beam | 9 |
| Figure 2.5 | Comparison of various experimental angular neutron distributions from Be(d,n) reaction using thick and thin beryllium targets | 9 |
| Figure 2.6 | SPERT B16/68 forced coolant flow transients: experiment and calculation | 11 |
| Figure 2.7 | Comparison of coolant pressure (calculation and experiment) as a function of time for a blowdown experiment | 13 |
| Figure 2.8 | Heater temperature (calculation and experiment) as a function of time for a blowdown experiment. | 13 |
| Figure 2.9 | (a) Variation of choking pressure with time: blowdown experiments<br>(b) Variation of vessel pressure with time: blowdown experiments | 14 |
| Figure 3.1 | $^{232}$Th fission fragment angular distribution for neutron induced fission at various neutron energies: experiment, calculations with two and three humped barriers | 23 |
| Figure 3.2 | $^{232}$Th fission cross section as a function of energy: measured and calculated | 24 |
| Figure 3.3 | $^{252}$Cf neutron emission as a function of fission fragment mass | 27 |
| Figure 3.4 | s- and p-wave radiative widths as functions of mass number | 28 |
| Figure 3.5 | (a) Initial state correlations between reduced neutron and radiative widths<br>(b) Ratio of calculated to measured valence widths as function of mass number | 30 |
| Figure 3.6 | The level density per unit mass as function of Cameron shell correction | 30 |
| Figure 3.7 | Capture yield for sodium as function of neutron energy | 32 |
| Figure 3.8 | Fits to the 118.8 keV resonance in $^{91}$Zr assuming g=1 and g=2 respectively | 34 |
| Figure 3.9 | Neutron transmission data for $^{91}$Zr taken at 80 m station, ORELA | 34 |
| Figure 3.10 | Cadmium partial capture cross sections obtained from measured neutron capture $\gamma$-ray intensity | 36 |
| Figure 3.11 | Unfolded spectra from 3d nuclei at various energies | 37 |
| Figure 3.12 | Differentiated gamma spectra obtained from gammas scattered from ancient bronze specimen | 41 |
| Figure 3.13 | Time of flight spectra for the F(p,$\alpha\gamma$) reaction are shown for various detector positions | 36 |

## 1. INTRODUCTION

The official Inquiry into Environmental Aspects of Uranium Mining by Mr. Justice Fox has had a major influence on this year's work. The reduction in uranium exploration expenditure has reduced demand for service work, much time has been spent providing information in connection with submissions to the Inquiry and it has had an unsettling effect on research. However, there has been a gratifying increase in the number of enquiries on the availability of nuclear techniques to solve industrial and research problems.

Cooperation with Oak Ridge National Laboratory on analysis and interpretation of neutron capture cross sections has continued. Scientific interest has continued to revolve around those isotopes with almost closed shell configurations. An additional capture mechanism of the single particle character over and above the valence capture mechanism is required to explain the observed correlations.

Much time has been devoted to finding Strutinsky barrier parameters which would provide an adequate description of both the fission cross section and fission fragment angular distribution of $^{232}$Th. A reasonably satisfactory quantitative fit was achieved using a three humped potential barrier. Nubar measurements for $^{232}$Th revealed no deviation from linearity with energy up to 1.6 MeV, and nubar measurements on $^{230}$Th failed to reveal the expected increase in nubar as the transition over the fission barrier was made. Improved measurements of neutron emission from $^{252}$Cf spontaneous fission fragments has confirmed the structure due to even-odd charge effects.

The study of SPERT transients was completed with calculations of the series of forced coolant flow transients. The physics of transient heat flow is now being examined. We have participated in the international comparison of calculations on Standard Loss of Coolant problems, using NAIAD. While Standard Problem 3 presented no difficulties, the reflooding aspects of the emergency core cooling in Standard Problem 4 presents major problems, i.e. thermodynamic non-equilibrium and the one-dimensional aspect of the code. Several promising lines of developments are in hand which, if successful, will remove these difficulties and will lead to a more versatile code.

Fairly intensive and increasing use is being made of the PDP-11/10 as an input/output terminal with interactive facilities. This has been successfully used to follow, visually, the progress of loss of coolant accidents and to provide interactive least squares analysis. A variety of applied spectral unfolding problems have been identified and tackled with these interactive facilities.

Information on the rainfall, run-off water and impurity concentration of run-off and spring water from White's tailings mound at Rum Jungle, is now becoming available from equipment installed there during the dry season. It is hoped that a self-consistent picture will emerge of water behaviour, and that this will assist in understanding the pollution problem. Codes have been developed to determine air and water movement within the heap.

## 2. REACTOR STUDIES

### 2.1 Moata

#### 2.1.1 Moata Operations (T. Wall)

Moata was operated on 72 per cent of all available working days for a 27 MWh fuel burn-up (cumulative burn-up 176 MWh). Principal uses of the reactor were uranium ore assay, fluorine assay and neutron radiography, with lesser periods for student training.

During the year, eight fuel element assemblies from the reactor core (96 plates) and 25 essentially unirradiated plates from storage were microscopically examined in the Hot Cells. Possible small defects were found on 10 plates from the core, and on one of the plates from storage. The suspect plates were replaced by fully inspected plates from storage before the elements were reassembled and returned to core. Four further core fuel element assemblies (48 plates) and 19 plates from storage remain to be examined. Normal reactor operation was maintained with minimal interruption throughout this exercise.

The suspected defects are still being given detailed study by Materials Division and, meanwhile, the frequency of routine monitoring of the Moata primary coolant $\beta^-$ activity has been increased. To date, all levels have been entirely compatible with $^{27}Al(n,\alpha)^{24}Na$ activation, and no fission product activity has been detected.

Uranium Ore Analysis

The table shows the work load on the Uranium Analysis Service since its inception.

| | 1974 | 1975 | 1976 (to Aug.) | Total to 1/8/76 |
|---|---|---|---|---|
| Samples analysed | 1424 | 4246 | 4744 | 10414 |

The demand on the service was such that a throughput of 320 samples per 8 hour day was achieved on several occasions.

A second uranium analysis rig for installation on HIFAR is under construction and should be ready for testing by the end of 1976.

Neutron Radiography

The routine neutron radiography of door thrusters for Qantas Airways continued, bringing the total number radiographed to over 100.

Neutron radiography of a microswitch commonly used in radio transmitters has revealed possible defects in the design. The switches had failed prematurely by short and open circuit faults. X-radiography did not establish the cause of failure. Neutron radiographs of the microswitches revealed variations of the epoxy based seating of the spring element from one switch to another, the location of the polymer damper and plunger. This information allowed the specification to be checked out. The likely cause of failure was judged to be the non-uniform seating of the spring element.

Characterisation of Obsidian

This work on obsidian volcanic glass was concluded with presentation of data on samples from several volcanic and archaeological sites, in a paper to the Melbourne Conference on Scientific Methods of Research on the Study of Ancient Chinese and South East Asian Metal Artefacts. The main tasks of the project were to demonstrate significant differences between trace element content of various sources of obsidian, and to relate trace element content of artefact obsidian to the original natural source. These aims were achieved by analysing irradiated obsidian for both long and short-lived isotope concentrations, but an attempt to characterise a source completely by short-lived isotope analysis only, followed by delayed neutron activation (uranium content) was only partly successful. The cost of the reactor time required to build up the long lived isotopes prohibits use of this technique for routine analysis of large numbers of samples. However, the technique is still likely to be useful for cases in which some artefacts are not completely identified by simpler nuclear analysis methods (section 3.5).

2.1.2 Fluorine neutron activation analysis (T. Wall, T. X. Bernold)

Measurement of the fast neutron induced reaction $^{19}F(n,\alpha)^{16}N$ is potentially a very useful and non-destructive means for assay of fluorine, an element difficult to assay by other standard techniques. The activation product $^{16}N$ decays by the emission of 6134 and 7112 keV gamma with a 7.4 s half-life. A fast sample transfer system moved activated samples from the reactor source to the counting station where a gamma spectrometer selects the very high energy gamma rays from other possible interferences. Using the P1 sample transfer facility on Moata and a germanium lithium drifted gamma ray detector, a set of samples covering 1 to 45 $^{w}/o$ fluorine and ranging down to as little as 10 mg total F content, has been analysed with a relative accuracy of ±4 per cent (coefficient of variation).

Present limitations to achieving better accuracy are:

(i) variation in sample travel time,

(ii) self-absorption in large mass and high density samples, and

(iii) thermal activation of the matrix causing gamma pile-up and loss of gain.

Limitation (i) can be overcome by construction of a transfer rig specifically designed for this type of application, (ii) by optimisation of counting geometry, and (ii) can be eliminated partially by using cadmium sample covers to reduce thermal activation. These two latter aspects are currently being investigated.

2.1.3 Moata Transients (D. B. McCulloch, J. W. Connolly)

Measurements in Moata of self-terminating reactivity transients with zero coolant flow were extended down to an initial period of ~15 s. Comparison of the results with the predictions of the ZAPP point kinetics heat transfer code (Figure 2.1) showed excellent agreement for the peak power reached, but the experimentally determined energy releases to the time of peak power were some 60 per cent higher than predicted by ZAPP. This was to be expected, since the ZAPP assumption of zero heat loss would not hold well for these slow transients.

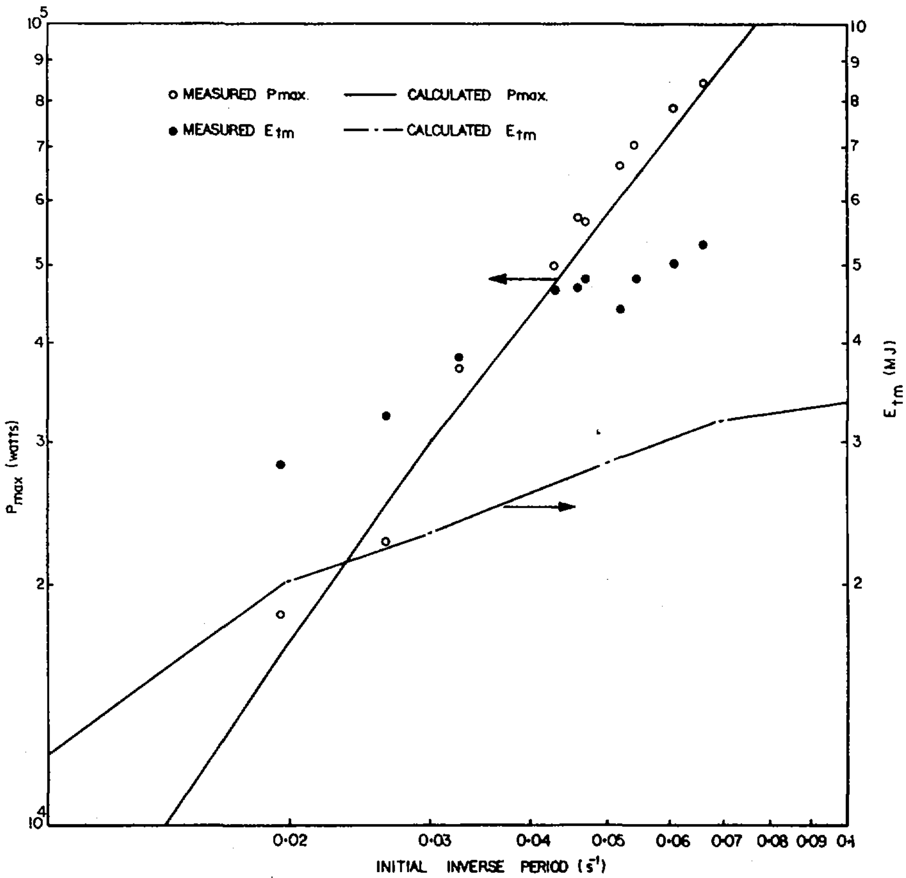


Figure 2.1 Moata transients: experiments and ZAPP Calculations

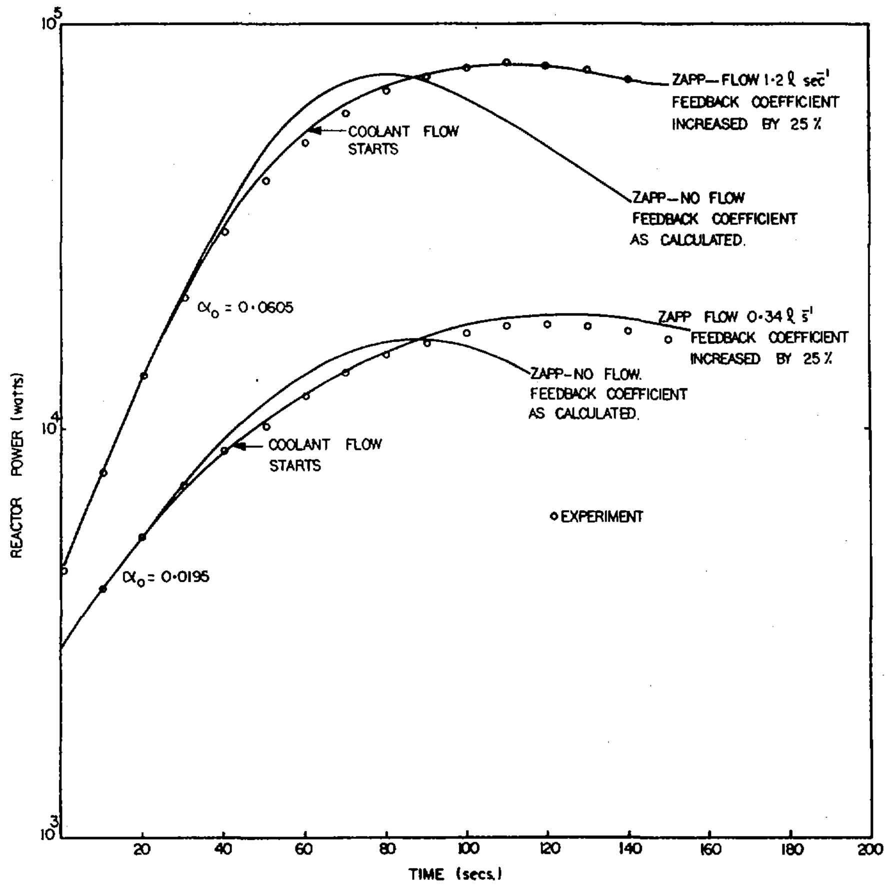


Figure 2.2 Moata transients: effect of coolant flow on power burst shape

The observed energy releases can be accounted for in terms of the observed onset of strong natural convective flow as peak power is approached. For one transient ($\tau_o$ = 16.5 s) a crude measurement of initial convective flow rate was made by placing two vertically separated thermocouples in the water reflector above the core. At a power level of about 55 kW, a temperature front was observed at the thermocouples, the time delay between the thermocouples suggesting a flow velocity of ~0.7 cm $s^{-1}$, or an initial flow rate of ~0.7 $\ell$ $s^{-1}$.

Inclusion of an ultra-simple constant convective flow rate model in the ZAPP calculations, with some reasonable empirical adjustment of the parameters (e.g. flow rate, power at which flow starts, flow reactivity feedback coefficient) sufficed to produce burst shapes in good agreement with those observed. This is illustrated in Figure 2.2.

2.2 Critical Facility (D. B. McCulloch, J. W. Connolly, J. R. Harries, G. Durance)

The experimental program on the hard spectrum core FC1 assembly (described in AAEC/PR41-P) was completed. Detailed calculations using the AAEC AUS code system with data derived from ENDF/B-IV are also now essentially complete. Comparison with the experimental data and preparation of a final report are in hand.

The excellent agreement reported earlier (see AAEC/PR41-P) between the experimental critical mass and that predicted by the preliminary design calculations (based on older AAEC-GYMEA data with nominal values of graphite density, etc.) has now been shown to have been somewhat fortuitous. Nevertheless, the overall agreement between the later, more detailed calculations and the experimental results, remains satisfactory (e.g. calculated $k_{eff}$/experimental $k_{eff}$ = 1.0075).

Cell flux fine structure has proved to be of greater significance than anticipated and has necessitated rather large corrections (typically ~10 per cent for the fission chambers) to the core region experimental reaction rates to convert them to 'cell-averaged' values. The corrected results agreed with the calculated axial reaction rate distributions to within ~8 per cent.

Work with this assembly has considerably widened our experience of the operational and experimental aspects of using the facility, which will be of considerable value in a future program. As a result, some modifications have already been made to the machine to improve operational convenience and experimental flexibility.

This period also saw the experimental capability of the facility considerably enhanced by the installation of a PDP-11/40 computer with interactive display facilities, and connected via the Dataway to the site IBM 360/65 central computer. The system is interfaced by CAMAC units to the nucleonic instrumentation of the experiments.

It has been intended to follow the FC1 assembly with small, polyethylene moderated core in which temperature and void coefficients of reactivity could be determined in core and reflector regions. It was expected that the data obtained would have some interest in the interpretation of SPERT experiments and perhaps in light water reactor safety studies. It was decided, however, that there was insufficient justification to proceed with this assembly pending a full review of the experimental program for the facility.

### 2.2.1 Reactor noise (J. R. Harries, R. B. Knott)

The reactor noise data from the Moata mockup assemblies have now been analysed to provide information on the coupling between the two core regions and the prompt neutron decay constants.

Theoretical prompt neutron lifetimes and effective delayed neutron fractions have been calculated using two and three dimensional diffusion codes. The two dimensional calculations predicted the observed trend of lifetime with core spacing, but a single model could not simultaneously predict satisfactory values for both the multiplication of the assembly and the prompt neutron lifetime. This arose from the difficulty of modelling the three dimensional features of the assembly in two dimensions. The calculations carried out using the three dimensional code improved the agreement between calculation and observation.

## 2.3 Pulsed Integral Experiments with Heavy Metal Assemblies

(A. I. M. Ritchie, M. T. Rainbow)

The unusual behaviour of the experimentally determined instantaneous decay constants of both $^{235}U$ and $^{239}Pu$ reaction rates in a thorium assembly, in which pulsed Li(p,n) sources were used, is still being investigated. The instantaneous decay constants vary quite markedly with time after the pulse and are quite different from the results of calculations. The experimental results were repeatable at the time of measurement. Recent repeat measurements made at a single spatial location in the thorium assembly have not been in agreement with those measurements made at the same location in the original experiment. Present indications are that the original experiments were subject to some unidentified influence.

A new series of measurements has been made of the time dependent $^{235}U$ reaction rate in the thorium assembly with a pulsed Li(p,n) source. During this series of measurements, the number of auxiliary measurements made to ensure the experiment is proceeding as expected, has been increased. The accelerator beam pulse profile previously monitored occasionally, is now measured continuously and the source neutron energy spectrum is now checked occasionally using a time of flight technique.

A quantity of depleted uranium (0.2 $^{w}/o$ $^{235}U$) has been acquired. Experiments with an assembly of this material will begin when experiments with the thorium assembly are completed.

Calculations with the code TENDS have been used to indicate the sensitivity of experiments to various experimental parameters. These calculations are used to clarify which parameters need to be closely controlled and to evaluate which are the most useful experiments to perform.

Of current interest is the information that might be obtained using the organic scintillator NE213 as a detector with a well defined neutron energy threshold, rather than as an energy spectrometer with good timing resolution.

2.4 Neutron Spectrometry (A. Rose, S. Whittlestone)

Three, 25 mm diameter, spherical detectors are available for routine use. These are filled with 1 atmos $H_2$, 3 atmos $H_2$ and 3 atmos $CH_4$ and enable users to measure spectra over the energy range 20 keV to 1.2 MeV. An indication of the accuracy that can be obtained using these detectors and the consistency of the results in the overlap region of the three detectors, can be obtained from Figure 2.3. This shows the neutron spectrum obtained by 2.8 MeV proton irradiation of a thick lithium target at $0^{\circ}$ to incident beam. This spectrum covers the energy range 0 to 1.1 MeV with a sharp cut-off at the high energy end, which is rounded off in Figure 2.3 by the resolution broadening of the detector.

An extensive series of measurements has been carried out on the angular distribution of the thick target Li(p,n) source, both to obtain expertise in the operation of these detectors and to obtain data on this source which is used in some current neutronics experiments. An inability to achieve consistent results at angles between $90^{\circ}$ and $60^{\circ}$ with slightly different target geometries, and to obtain the same good level of agreement with calculated spectra that had been noted at other angles, has been traced to the effect of the scattering resonance in $^{7}Li$ at ~250 keV. Since neutrons are generated at the front face of the target, those emitted at angles between $90^{\circ}$ and $60^{\circ}$ pass through the maximum thickness of lithium which, for most of the target geometries used, was a significant fraction of a mean free path for neutrons with the resonant energy.

Further work has continued on the development of small (~0.5 $cm^3$) detectors filled with the liquid scintillator NE213, whose good timing resolution will allow time dependent neutron energy spectra to be measured in the pulsed heavy metal assemblies. Details of this development work are given in §4.3, but the following are the major points of interest. Replacement of the perspex light guides by quartz light guides has increased light transmission from the detector chamber from 25 per cent to 80 per cent. A change in the shape of the detector chamber has produced a further 30 per cent increase in the light output. These improvements make it likely that spectra can be measured with good accuracy down to neutron energies of 200 keV.

Neutron Energy Spectra from the Thick Target Be(d,n) Source

The $^{9}Be(d,n)^{10}Be$ reaction is a prolific source of neutrons with energies in the MeV range when the deuteron energy is limited to about 3 MeV, a common limit for many charged particle accelerators. The excellent chemical and mechanical properties of beryllium make this source ideal for many neutronics and neutron irradiation studies. However, the neutron energy spectrum is complex because of the many energy levels available to the $^{10}Be$ residual nucleus and details of the angle depenent neutron energy spectrum are necessary for interpretation of many neutronics experiments, including some in progress at Lucas Heights.

Motivation for a comprehensive set of measurements on the angle dependent energy spectra associated with this source arose, in part, from a single measurement carried out at Lucas Heights, which proved to be in considerable disagreement with the only

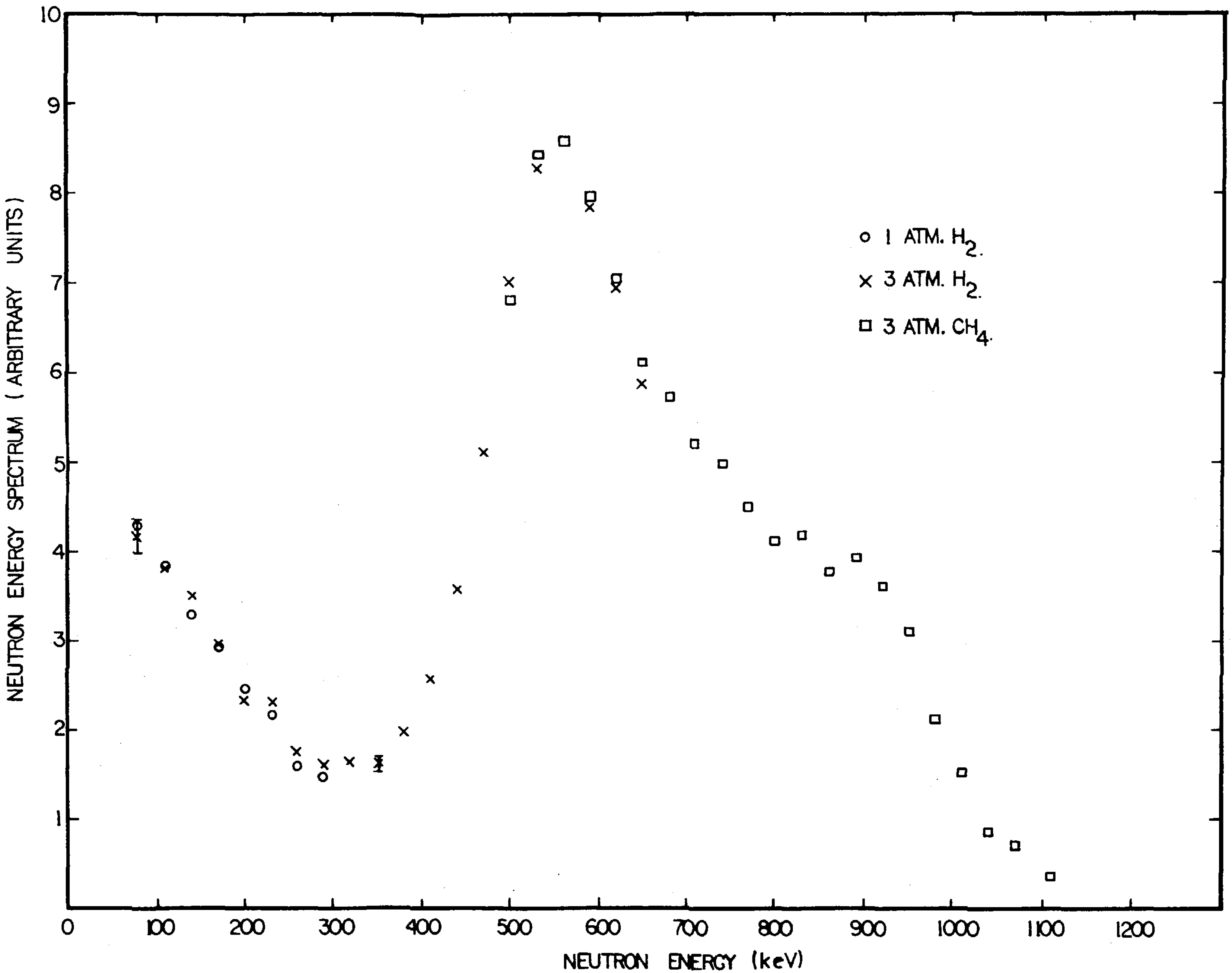


Figure 2.3 Neutron energy spectrum from 2.8 MeV proton irradiation of a thick lithium target at $0^{\circ}$ to the incident beam

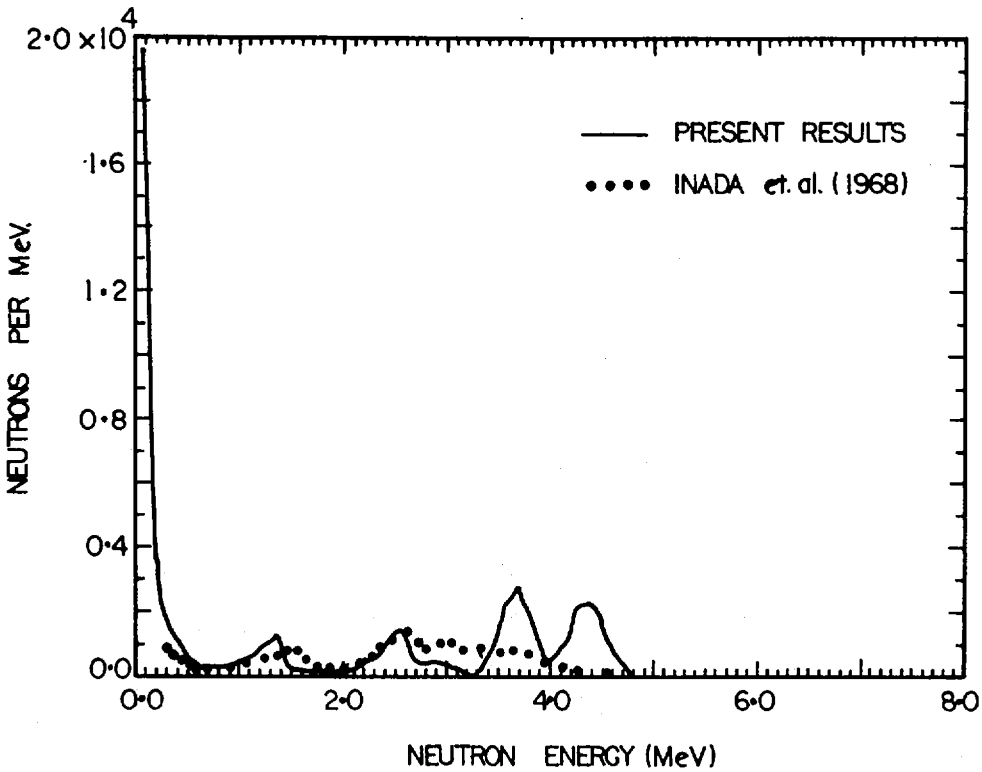


Figure 2.4 Neutron energy spectrum from 1.4 MeV deuteron irradiation of beryllium at 150° to incident beam

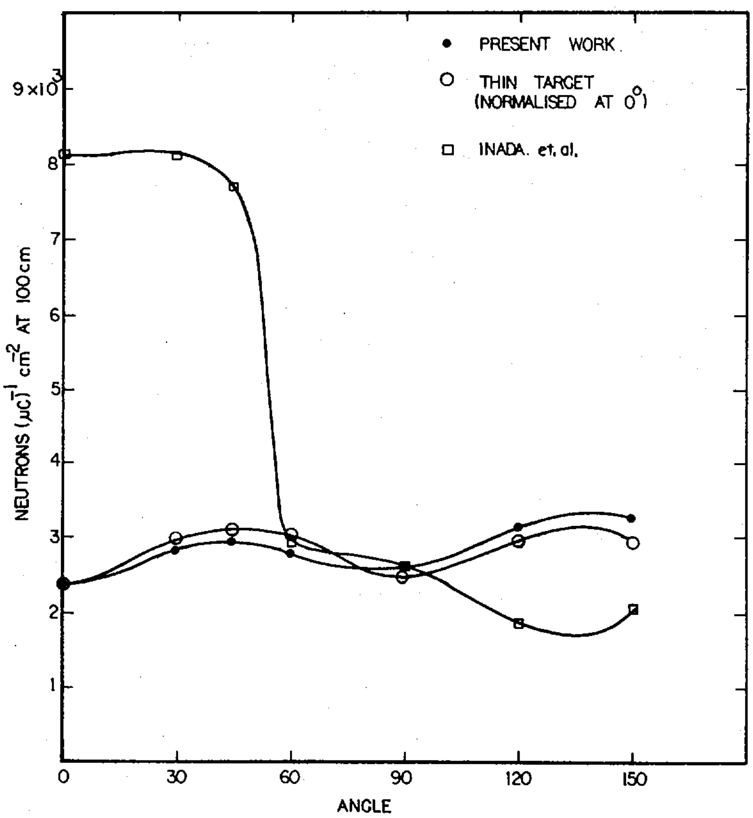


Figure 2.5 Comparison of various experimental angular neutron distributions from Be(d,n) reaction using thick and thin beryllium targets

other comprehensive measurement quoted in the literature (Inada et al. 1967)* and in part from the availability of highly sensitive neutron detectors of known efficiency from the work on liquid scintillation detectors.

Neutron energy spectra have been measured at angles of 0, 30, 45, 60, 90, 120 and 150$^{o}$, and for deuteron energies of 1.4, 1.8, 2.3 and 2.8 MeV. Figure 2.4 shows a fairly typical spectrum which was obtained at 150$^{o}$ and 1.4 MeV, together with the corresponding result of Inada et al. It can be seen that while the two results have features in common, the present results have considerably better energy resolution.

The major disagreements between the present results and those of Inada et al. appear in the shape of the angular distribution where Inada et al. find much greater forward peaking. Some thin target angular distribution measurements by Siemssen et al. (1965)† were used to estimate thick target angular distributions. These are shown in Figure 2.5, where it can be seen that they are in much better agreement with the present results than with those of Inada et al.

In this context it should be noted that a comparison of calculated and measured spatial distributions in the pulsed thorium assembly with a Be(d,n) source indicated that the calculated results showed more forward/backward asymmetry than was apparent in the experimental results. The source distribution used in those calculations was that due to Inada et al.

## 2.5 Reactor Safety Studies

### 2.5.1 Calculation of SPERT transients - forced coolant flow (J.W. Connolly)

The experimental program for core B18/68 included a number of power transients initiated under conditions of forced coolant flow through the core. Flow velocities ranged from 0.12 m s$^{-1}$ to 4.3 m s$^{-1}$ giving transit times for the coolant to traverse the core of 5 s to 0.14 s. A very simple model to represent coolant flow was incorporated in ZAPP in an attempt to calculate these transients.

The flow model transfers material from a specified region of one axial zone of the reactor representation to a specified region of another, at a rate corresponding to the flow velocity given in the code input data. The material moved has the average temperature of the region from which it comes, and is mixed uniformly with the material of the destination zone. Heat transfer from the fuel plate to the coolant was assumed to be by conduction across a static film of water 0.03 mm wide. The conductivity of the remaining coolant was given the value unity to force a nearly flat temperature profile across the channel.

Figure 2.6 shows the results of calculations using the above model for transients of initial period 100 ms and a range of coolant flow rates. As the flow rate is increased, the average post-burst power level and the frequency of the secondary oscillations increase, primarily a result of the rate of energy removal from the core. Although the calculations do not correctly describe the amplitude and frequency of these oscillations, the general level of agreement with experiment is

---

*Inada, T., Kawachi, K. and Hiramoto, T. (1968) - J. Nucl. Sci. Tech. 5, 22

†Siemssen, R. H., Cosock, M. and Felst, R. (1965) - Nucl. Phys. 69, 209.

surprisingly good, particularly since the same static boundary layer thickness was used for all flow rates. (Trial runs of ZAPP showed that the thickness of this layer needed to be increased fourfold before serious divergencies from experiment were produced.) Calculated fuel plate temperatures for these transients were also in good agreement with experimental values.

A study has been made of hypothetical power excursions in HIFAR. Preliminary results suggest that loss of a CCA blade can be tolerated for critical angle >14$^{\circ}$. A report is in the course of preparation.

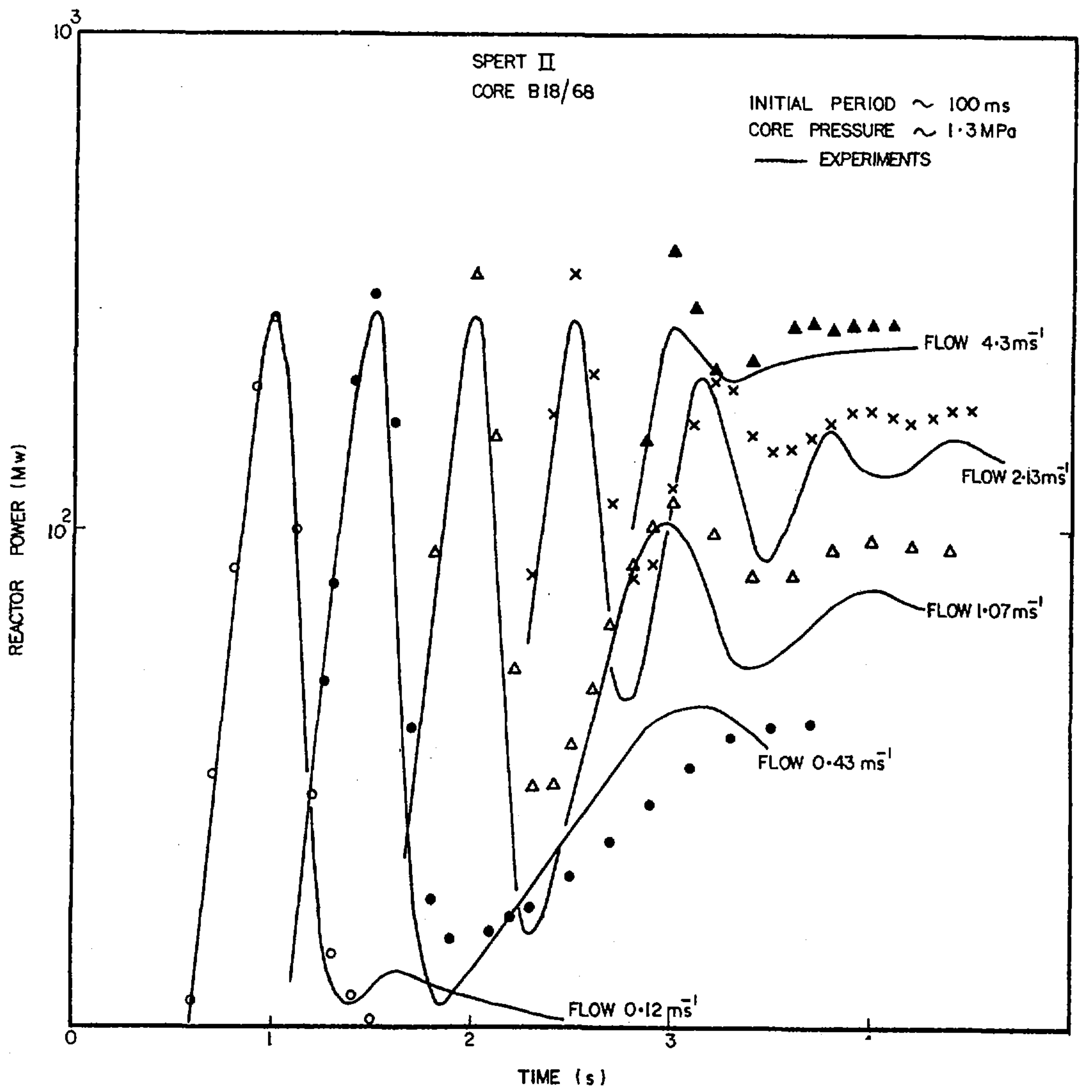


Figure 2.6 SPERT B16/68 forced coolant flow transients: experiment and calculation

2.5.2 LOCA analysis (W. J. Turner, G. D. Trimble, A. W. Dalton)

The OECD-NEA/CSNI in 1973 established a Working Party on Emergency Core Cooling, which has formulated a series of standard problems based on experiments, to be solved by each participating group using their own method of analysis. All solutions are subsequently compared with the experimental data.

Australia has joined this Working Party and Standard Problem No. 3 has been analysed using the NAIAD blowdown code. This experiment was a blowdown of the IETI-1 rig (CISE 1971*) from slightly subcooled conditions at the feeder inlet. This rig simulates the conditions in a single power channel of a pressure tube reactor. The transient was initiated by closing valves at the feeder inlet and riser outlet and opening a simulated break near the feeder inlet. During the transient, the flow reversed and dryout occurred over most of the heated section. Simulated power to the channel was continued for 12.3 s and measurements taken up to 18.5 s.

Comparisons of some calculated and measured parameters are shown in Figures 2.7 and 2.8. Figure 2.7 shows the pressure 8 cm upstream of the break, while Figure 2.8 shows the heater temperature at about the middle of the heated section.

Attention has been given to the effect of slip on the one dimensional conservation equations. These equations must remain hyperbolic or else they become physically meaningless. Detailed analysis of these equations over the entire range of pressure, enthalpy and mass velocity which can occur in transient situations, has been performed and has shown that all the commonly used slip models lead to non-hyperbolic equations for at least some of this range. This is generally because, in transient situations, the models are being extrapolated into areas beyond those for which they were originally formulated, there being little or no fundamental experimental data in these regions.

NAIAD has also been used to model a series of blowdown experiments done by the Engineering Division† at the AAEC. In these experiments, a range of hot, pressurised water/vapour systems were blown down through an orifice (choke flow), the blowdown being initiated by the rapid bursting of a disc downstream of the orifice. The results of the NAIAD calculations were compared with the measured pressures in the pressure vessel and at the choking point. Preliminary calculations indicate that reasonable agreement is obtained over the full duration of the blowdown transient. The comparison for an initial water/vapour ratio of 0.85 is shown in Figure 2.9.

This preliminary NAIAD representation will now be refined to provide closer simulation of the experimental conditions and should then provide improved agreement with the measured data. Among the refinements to be included are:

(a) Transfer of heat stored in walls of the pressure vessel and flanges to the liquid phase during the transient.

(b) Restriction of flow out of the pressure vessel by the heater situated at the outlet (whose function is to raise pressure within the pressure vessel to the required value prior to blowdown).

---

*CISE (1971) - Heat transfer and fluid flow studies. CISE Documentation Service, Milan, Italy.

†Holland, P. G. and Marshall, J. (1975) - AAEC/ER/UN76

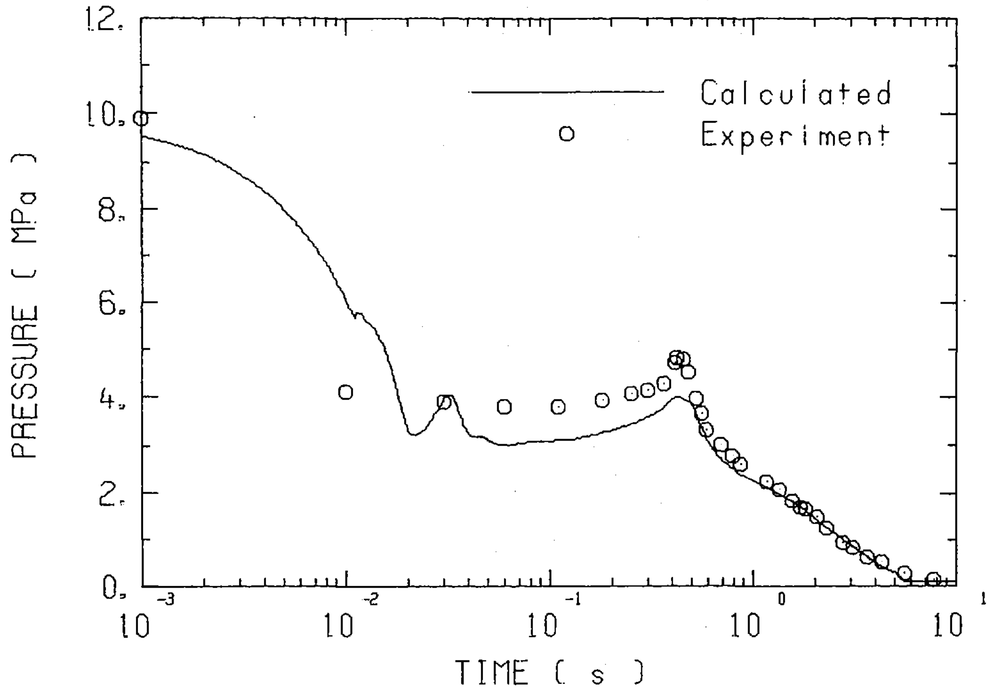


Figure 2.7 Comparison of coolant pressure (calculation and experiment) as a function of time for a blowdown experiment

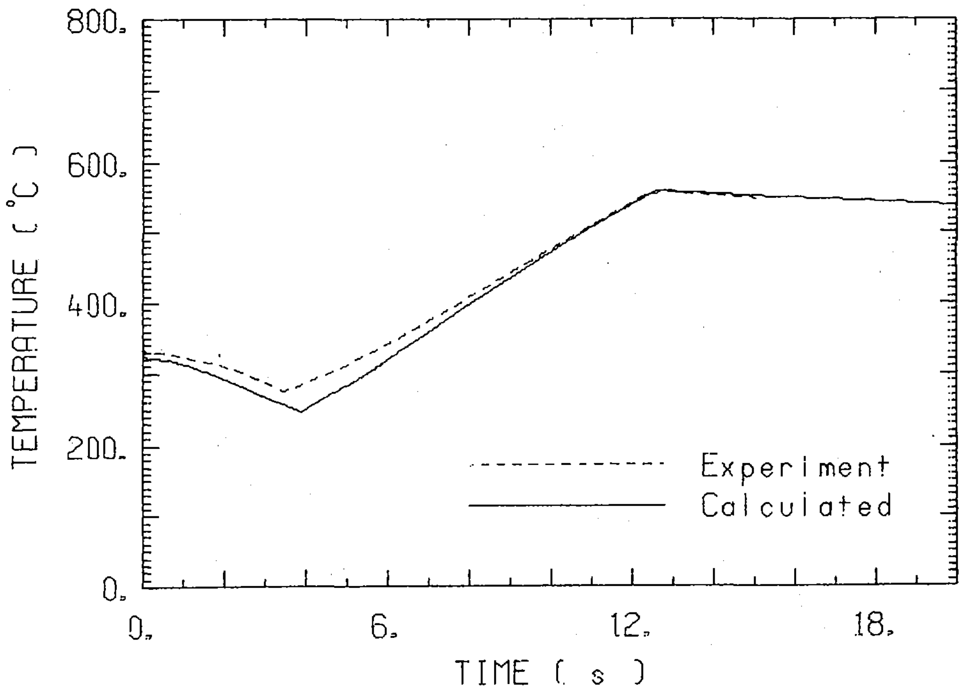


Figure 2.8 Heater temperature (calculation and experiment) as a function of time for a blowdown experiment

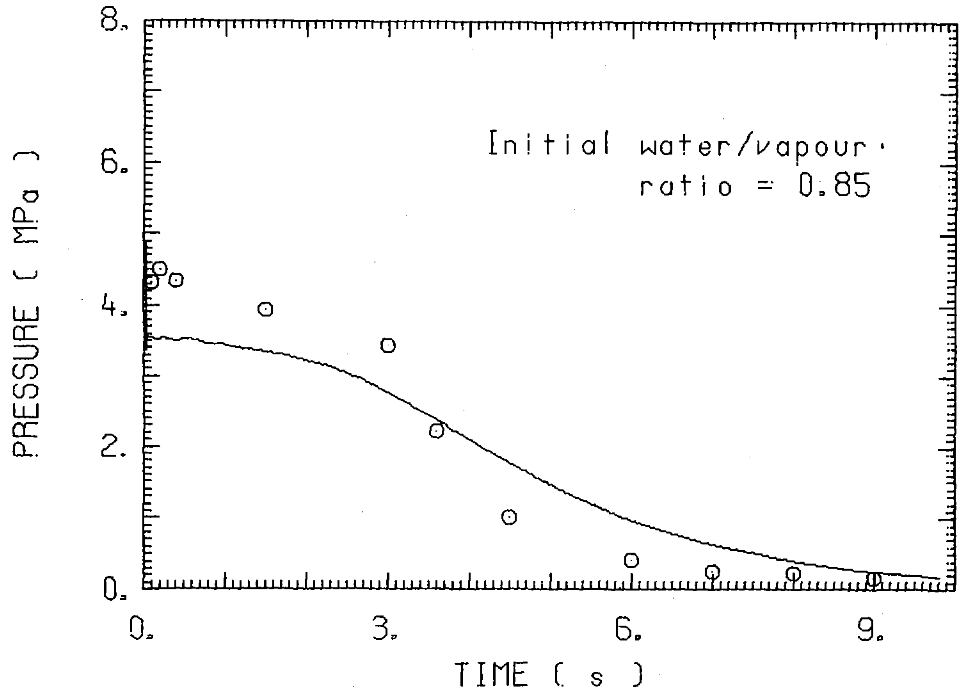


Figure 2.9 (a) Variation of choking pressure with time: blowdown experiments

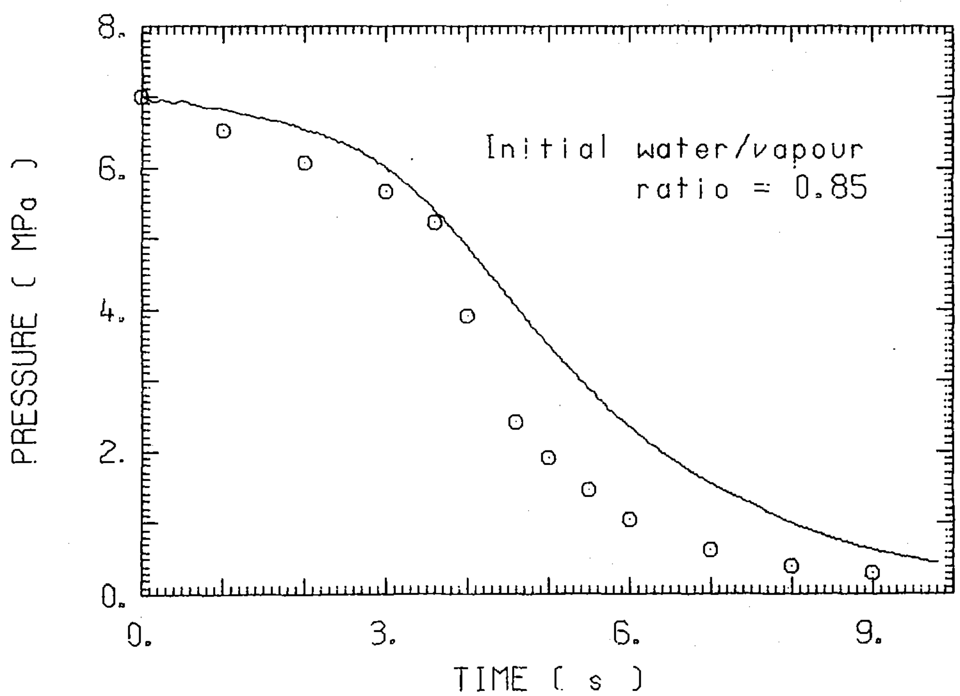


Figure 2.9 (b) Variation of vessel pressure with time: blowdown experiments

(c) Improvement of choke flow treatment.

Development of the NAIAD code has continued with the following improvements incorporated:

1. The equation of state routine has been rewritten to improve the sub-cooled liquid region. Special purpose tables with very high accuracy in particular regions may be generated as data for this routine, although the standard tables cover the entire pressure-enthalpy range with good accuracy.

2. An improved pump model has been added which accepts head, torque and two-phase difference data for up to five pumps and can handle shaft reversal and pump coastdown situations.

A detailed report of the code has been produced and distributed internationally and as part of the continuing Canadian interest in NAIAD, Dr. R. P. Collier of Atomic Energy of Canada Limited, visited the AAEC for three months to learn to use the code and has taken a copy of the code to Canada.

A description of the NAIAD code, together with the results of a calculation of a British blowdown experiment, were presented at the Specialists' Meeting on Transient Two-Phase Flow, held at Toronto, August 1976. As part of the presentation, a ten minute motion picture of the results was shown. This film was taken directly from the screen of Physics Division's GT40 computer using a dynamic display program that forms part of the NAIAD output analysis software.

### 2.5.3 Fission product decay energy (R. B. Knott)

The increased interest in the safety aspects of nuclear power reactors has led to renewed efforts on the calculation of fission product decay energy as a function of time after shutdown for a typical fuel element irradiation time history. The results of a survey suggest that in the time interval up to 100 s after shutdown, the data are not reliable.

The large uncertainties attached to the decay energy function are due to the inability of summation calculations to account for all the short-lived fission products. The solution to this problem is that short half-life pseudo-fission products are necessary. These may be obtained by comparing summation calculations with integral data from benchmark experiments. The available experimental data have large errors attached to the individual experiments and exhibit large inconsistencies between different experiments.

It was concluded that due to recent advances in experimental techniques, considerable improvement in the experimental data could be made.

## 2.6 HIFAR

### 2.6.1 HIFAR Dynamics (J. R. Harries, D. J. Wilson)

Realistic estimates of the response of HIFAR to reactivity or coolant flow transients can only be made if the time response of the power coefficient is known. An experiment to measure the time response has been carried out for negative reactivity transients produced by closing the secondary coolant valves at the inlet to the heat exchangers. The reactor power and the coolant temperature were recorded at 0.5 s intervals during the resulting transient.

The reactivity as a function of time during the transient was calculated from the power changes using an inverse kinetics code. Since the coarse control arms were not moved, the reactivity changes must be due to changes in temperature and xenon poisoning. The poisoning component was calculated from the observed power level and subtracted from the total reactivity. The residual reactivity change closely matched a temperature consisting of the fuel inlet temperature plus 78±8 per cent of the temperature rise through the core. No measureable time delays were observed. In the context of the experiment, this means that any delays were less than ~2 s.

On the basis of these results, a reactor dynamics code has been developed that combines the neutronic response of the reactor with the primary coolant circuit and heat exchanger characteristics.

### 2.6.2 X-170 rig support (D. J. Wilson, T. Wall)

A foil irradiation experiment has been successfully carried out using a special X-170 fuel pin to establish the relationship between pin fission rate and the ionisation current from a special movable fission chamber located close to the X-170 position in HIFAR. The calibration data will enable the power and burn-up of standard fuel pins in X-170 experiments to be monitored continuously via the fission chamber output.

### 2.6.3 Criticality (D. J. Wilson)

A comprehensive set of detailed calculations is in progress to assess the criticality safety of all storage locations on site, which may be used for HIFAR 170 g fuel elements.

2.7 Deep Ocean Currents and the Disposal of Radioactive Waste into the Ocean (J. R. Harries)

Low-level radioactive waste is being disposed of in the Atlantic Ocean by several European countries. Japan is currently making feasibility studies for disposal of low-level waste into the Pacific Ocean. At present, the internationally agreed disposal limits, which are considerably above any currently contemplated disposal program, are derived from a simple diffusion model which assumes an ocean of infinite horizontal extent, and ignores any bulk transport of water.

A study is being made of the deep circulation in the oceans, beginning with the Coral and Tasman Seas and subsequently extending out into the Indian and Pacific Oceans. Using published data for the Tasman and Coral Seas, an advection-diffusion model has been constructed for the transport of water from the deep Tasman Sea to the surface near Antarctica.

2.8 Assistance to Indonesia (P. Duerden, B. Harrington)

Australian assistance was sought for a nuclear radiation measurement project at the Pusat Reaktor Atom Bandung. This has now been completed. Two Indonesians were attached to Lucas Heights for an initial training period and to assemble, test and calibrate the necessary specialist equipment under our supervision and using AAEC's facilities. The actual measurement program subsequently took place at the TRIGA MK II (uranium-zirconium hydride pool type) reactor in Bandung, Indonesia, supervised by an officer of Physics Division's staff. The project was concerned with relative and absolute neutron flux measurements, neutron energy spectrum characterisation, flux scanning with self-powered neutron detectors, and measurement of fast neutron and $\gamma$-ray dose rates with Neary type ion chambers. Reactivity worths of various foil materials and reactivity changes due to fuel element replacements were also measured.

The flux and spectrum measurements used a large number of different activation foils. Cadmium ratio measurements to give the neutron spectrum index $r\sqrt{T/T_o}$, and absolute measurements of thermal neutron flux were made for various locations in the reactor. A platinum and a rhodium self-compensated, self-powered neutron detector (SPND) were used for scanning the relative flux vertically in the reactor.

The Neary ion chambers were designed to measure the dose from fast neutrons and gamma radiation. One of them has a wall material composed of a fused mixture of finely divided graphite, polyethylene and polystyrene, the ratio of carbon and hydrogen in the mixture being 12:1 by weight; it is filled with acetylene. This chamber registers the sum of the fast neutron and gamma radiation. A second chamber, with the same dimensions, has a wall of magnesium, a gas filling of argon and measures the gamma radiation only. The chambers were fabricated and calibrated at Lucas Heights and are intended for routine measurements of fast neutron dose in a rice irradiation facility in the reactor.

Physics calculations for the TRIGA reactor have been made at Lucas Heights. Parameters calculated include power maps, activation rates and reactivity worths across the core for the various foil materials used experimentally, and fuel element reactivity worths as a function of burn-up.

Comparisons between most of the experimental data and calculation have been completed, but the fuel element reactivity worth experiments are proving very difficult to interpret because the reactivity worth of each of the four control rods of TRIGA is very dependent upon the positions of the other three rods.

2.9 Neutron Source Project (G. Hogg, J. Tendys, J. Daniel)

The characteristics of a small dense plasma focus device have been investigated. The inner electrode diameter is 2.5 cm and various outer electrode configurations, such as rods, solid and perforated cylinders (diameters to 8 cm) have been used, together with various insulator lengths. The neutron output has been measured as a function of capacitor bank voltage (16-25 keV equivalent to a bank energy of 1-2.5 kJ) and deuterium gas filling pressure (10-1000 Pa). Neutron output varies as the square of the voltage applied to the device itself. The maximum single shot neutron output that has been measured for this small gun is $4 \times 10^7$. However, the neutron output is variable and for the conditions of the peak shot, the average yield over 25 shots was $1.2 \times 10^7$ neutrons. A major problem has been the reduction of the inductance of the device header and the cable system, so that more than half the capacitor voltage is applied to the gun itself (gun inductance ~25 nH).

## 3. NEUTRON PHYSICS

### 3.1 3 MeV Accelerator (A. van Heugten, H. Broe, J. Fallon, M. Kenny)

The accelerator was used for 3981 hours during the year from July 1, 1975 to June 30, 1976. Time allocation for the various experimental projects is shown in Table 3.1. In January, the accelerator passed 50 000 hours of operation, accumulated during the 11 years since its installation. Unattended running was used extensively during the year without any problems.

No major breakdowns occurred during the year, although intermittent trouble was experienced with the RF pulsing system. The terminal circuitry for switching between beam modes was completely rewired and simplified. Power supplies for microsecond pulsing were changed over to solid state components. A new beam current integrator system was installed.

#### Data Acquisition Facilities
(M. D. Scott, R. J. Cawley)

The PDP7, formerly the principal data acquisition facility for all major accelerator experiments has, after 10 years, been supplanted by the PDP15, thereby removing a long-standing constraint on capacity and flexibility.

Utilisation of the expanded PDP15 was, at first, frustrated by severe hardware problems associated with the interleaving of direct memory access I/O transfers, such as are used by the site Dataway and PDP7-PDP15 link interfaces, with central processer cycles employing the Ampex memory or the CAMAC interface. Failures were also observed under some conditions with programs running in the standard Digital Equipment Corporation (DEC) memory and using the extended arithmetic element (EAE).

Techniques were developed for reproducing such intermittent fault conditions and the cause traced to design inconsistencies in the I/O processer of the PDP15 itself.

With the assistance of Digital Systems Group and the use of a logic analyser, particular failure sequences were investigated one by one, with a view to devising appropriate modifications to the I/O processer. The best result was obtained by replacing the I/O processer clock with a signal synchronised to central processer unit (CPU) operations. In this condition, no complete hangups occur in any I/O mode; the site Dataway interface now functions under all conditions, but the PDP7-PDP15 link still malfunctions intermittently. At this point, the system was pronounced usable and belatedly put in to service with software and procedural measures to avoid PDP7-PDP15 link failures.

New user programs have been developed to take advantage of the addition of 24K of Ampex core memory and the EAE recently installed on the PDP15.

SDIG15: A two parameter digital window program with approximately 22K of data storage area. The storage area varies according to the size of the monitor spectrum and its corresponding digital window table. The program incorporates light pen spectrum stripping, channel number to energy conversion, time of flight channel number to energy conversion, spectrum dumping and retrieval to a IBM360/65 disk

TABLE 3.1

ACCELERATOR TIME ALLOCATION - JULY 1, 1975 TO JUNE 30, 1976

| Category | Experiment Title | Personnel | Origin | Running Time (hours) |
|---|---|---|---|---|
| Neutron Data | | | | |
| Fission | $\bar{\nu}$ versus Neutron Energy | Boldeman, Walsh | Neutron Physics | |
| | Fragment Angular Distribution | Caruana | Wollongong | |
| | $^{252}$Cf | Culley | Expt.Reactor Physics | 1012 |
| Capture | Capture $\gamma$-ray Spectra | Kenny, Allen | Neutron Physics | |
| | | Pe | UNSW | |
| | | Taylor | James Cook Univ. | 885 |
| Neutron Transport | Pulsed Integral - thorium | Rainbow | Exp.Reactor Physics | |
| | Pulsed Spectra - thorium | Whittlestone | Exp.Reactor Physics | |
| | Spectra - fast assemblies | Rose | Exp.Reactor Physics | 935 |
| Elemental Analysis | Oxygen Analysis | Bird, Russell, | Neutron Physics | |
| | Scanning | Scott | | |
| | Obsidian Analysis | Ambrose | ANU | |
| | Glass Analysis | Owen | ACI | |
| | Gas Flow | Allen | Neutron Physics | 947 |
| AINSE Projects | Crystals | Anderson | UNSW | 29 |
| | Channelling | Szpitalak | UNSW | 42 |
| | (p,$\gamma$) Spectroscopy | Lasich | Queensland Univ. | 27 |
| | Neutron Detector Calibration | Bartle | ANU | 104 |

| | |
|---|---|
| Total operating time | 3981 hours |
| Maintenance and development | 1522 hours |
| Unused time | 2709 hours |

library, as well as all the features offered by the simpler PDP7 program DIGWIN.

FOCAL15: Developed for single parameter pulse height analysis work. The original DEC FOCAL system (supplied without source) was disassembled in order to obtain a skeleton source listing and this formed the basis for the expanded and modified FOCAL15 now in use. Approximately 50 commands were added to the FOCAL repertoire, mainly oriented towards experiment or display control and a spectrum display routine was also added. The original program was also modified to operate with the local supervisor program and error halts were removed so that the user's FOCAL program continued on after printing error messages.

As an aid to automatic experiment sequencing, a special exit routine, which responds to a predetermined CAMAC interrupt, was devised. This routine inhibits the CAMAC CRATE, thus effectively stopping data acquisition and any FOCAL operation in progress. It then starts execution of the user's stored FOCAL source, beginning execution at line 99.99. The user's FOCAL source may then perform analysis of the data, order printouts, etc., and may use CAMAC devices to change targets or perform other experimental control operations before restarting the experiment. Unattended experiment control in this fashion is already in operation.

General: The PDP7-PDP15 link operation causes program failure (due to incorrect link operation) if the link operation catches the program in AMPEX core or performing a CAMAC operation. A partial solution to this was to modify the PDP15 supervisor to hold control within the interrupt processer while LINK operations are in progress. However, this does not completely overcome the problem, as the PDP7 can asynchronously perform LINK operations when the PDP15 does not expect them. To further improve matters, the user is advised to disable the display and to avoid CAMAC operations when he is using the LINK to read or punch paper tape.

## 3.2 Fission Studies

### 3.2.1 Measurement of $^{252}$Cf fission neutron spectrum (D. Culley)

A knowledge of the energy distribution of fission neutrons is basic to reactor neutronics calculations. In an endeavour to improve the accuracy of these data, measurements are being made on $^{252}$Cf which has a fission half-life of 2.63 years.

The energies of the fission neutrons are measured by determining the flight time over a measured distance, using the event in the fission chamber as a start signal and the pulse in a neutron detector as a stop signal. The time of flight system is set on a tower, well above the ground, to minimise the backgrounds due to scattered neutrons.

Preliminary results have been obtained which have been used to test the analysis program written to convert time of flight measurements to energy spectra. The program determines relativistically correct energies and interpolates detector efficiencies from supplied data, for each channel of the time spectrum.

A major source of error is the determination of the efficiency of the neutron detectors. Many experimenters in the past have relied solely on calculations which may be in error by up to 5 per cent. In the present case, it is intended to combine calculation with ahsolute determination, using a 'proton telescope'.

The efficiency, $\varepsilon$, of the telescope is given by:

$$\varepsilon = M \cdot P\sigma_T(E)$$

where P is the number of hydrogen atoms $cm^{-2}$ of the radiator,
$\sigma_T(E)$ is the n-p scattering cross section at energy E,
M is a triple integral over telescope-source and radiator detector geometries.

A program has been written for the IBM 360/65 which reproduces the previous values of M to one part in $10^4$ and allows calculations at energies not quoted previously. Measurements of efficiency are being carried out using ac elerator produced neutron beams with specific energies.

### 3.2.2 Fission fragment angular distributions for $^{232}Th$

(J. Boldeman, R. Walsh)

In recent years there has been considerable difficulty in reconciling calculations of the fission barrier parameters for the thorium isotopes with those deduced from the experimental data. For example, in neutron fission of $^{232}Th$ analysis of the fission fragment angular distributions for fission through the $\beta$ vibrational band in the intermediate well (at 715 keV) indicated similar heights for the two humps of the fission barrier with a fairly shallow intermediate well*. A calculation of the fission barrier shape, using the Strutinsky prescription, suggested a considerably higher outer barrier with a fairly deep intermediate well. However, Möller and Nix** have recently shown that if mass asymmetric deformations are included in the calculation of the fission barriers, then for nuclei with $N < 146$ the outer barrier splits into two separate peaks with the potential energy surface now exhibiting a third minimum. The fine structure seen in their measurements of the neutron fission cross section of $^{232}Th$ has been interpreted by Blons et al.† as experimental evidence for this third minimum.

Historically, there has always been a considerable problem in reconciling the neutron fission cross section and angular distribution in neutron fission of $^{232}Th$. We have measured the fission fragment angular distribution for neutron fission of $^{232}Th$ at a number of energies near the nominal fission threshold. Previously, attempts had been made to obtain a simultaneous description of the fission cross section and the angular distribution with a single-humped fission barrier. In the present study, we have made a comprehensive but unsuccessful search for such a set of double-humped barrier parameters, which would describe the fission cross section and fission fragment angular distribution. However, a reasonably successful fit to the angular distribution and the neutron fission cross section was achieved using parameters for the triple-humped fission barrier model. The fit to the fission cross section and the angular distribution are shown in Figures 3.1 and 3.2 for both two-humped and three-humped barrier descriptions. The principal problem that remains is the large number of vibrational bands required in the third well to obtain the fits

---

*James, G. D., Lynn, J. E. and Earwaker, L. G. (1972) - Nucl. Phys. A189, 225
**Möller, P. and Nix, J. R. (1973) - Proc. 3rd IAEA Symp. Phys. and Chemistry of Fission, Rochester, Vol. 1, p. 103.
†Blons, J., Mazier, C. and Paya, D. (1975) - Phys. Rev. Letts. 35, 1749.

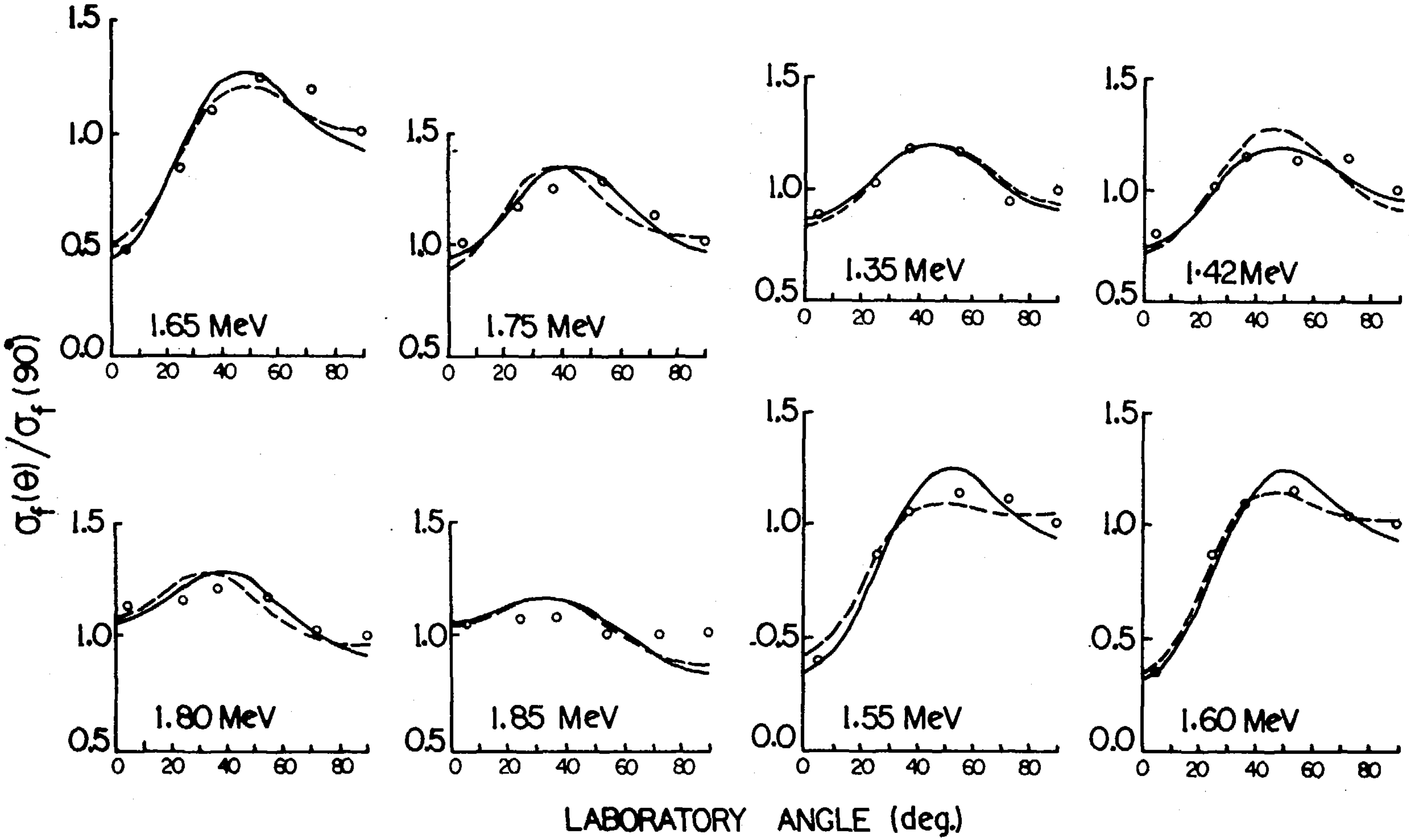


Figure 3.1 $^{232}$Th fission fragment angular distribution for neutron induced fission at various neutron energies: experiment, calculations with two and three humped barriers.
Two humped fission barrier indicated by solid line.
Three humped fission barrier indicated by dotted line.

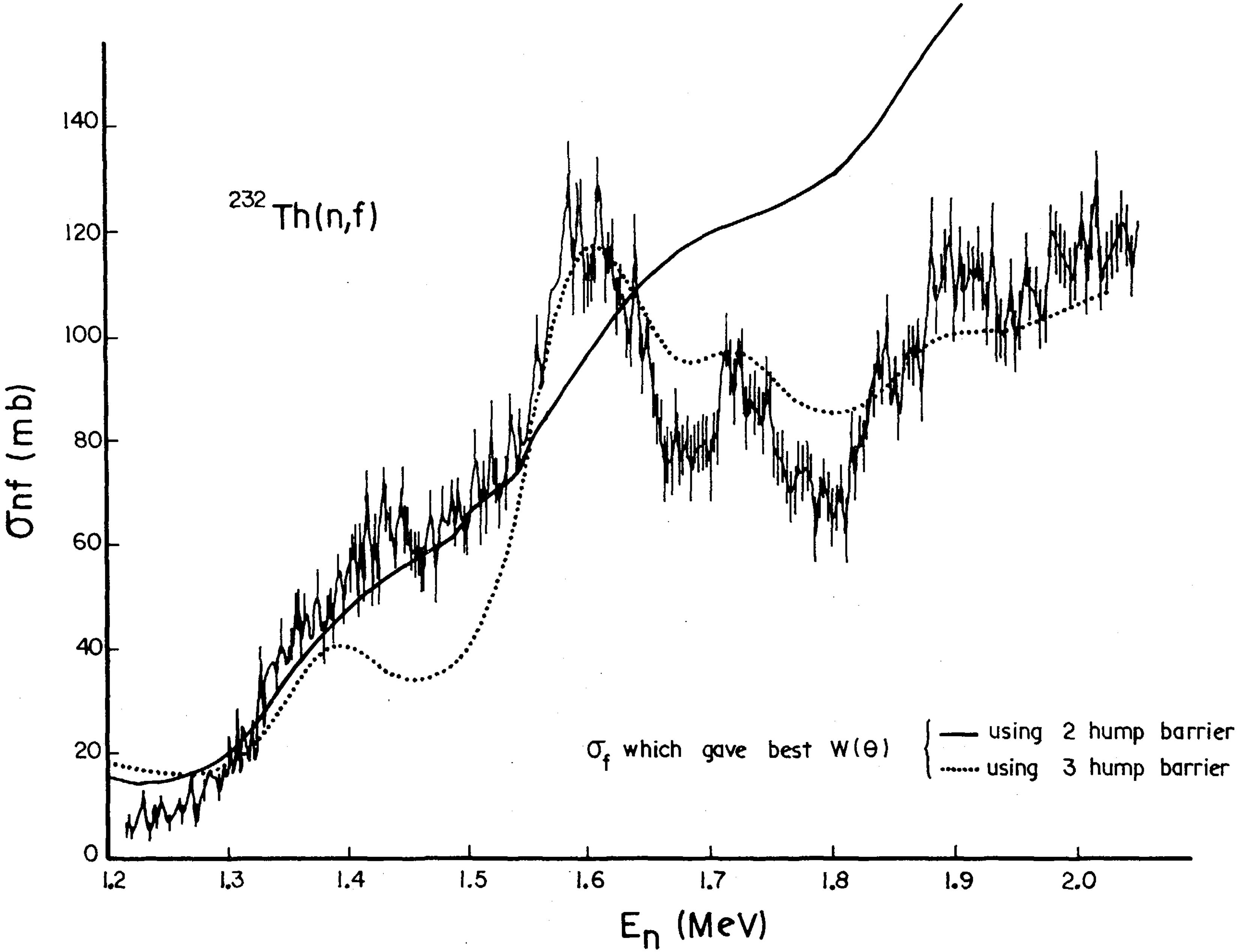


Figure 3.2 $^{232}$Th fission cross section as a function of energy: measured and calculated

shown in the figures. At present damping in the third well is being introduced into the calculations in an endeavour to reduce the number of vibrational bands required.

### 3.2.3 $\bar{\nu}_p$ measurements for neutron fission of $^{232}Th$ (J. Boldeman, R. Walsh)

To supplement the above studies, measurements of $\bar{\nu}_p$ (the average number of prompt neutrons emitted per fission) have been made for neutron fission of $^{232}Th$ near the fission threshold. Konchin and Manero* have reported the possibility of a large peak in $\bar{\nu}_p$ at or below a neutron energy of 1.4 MeV. Our measurements show no such peak, although a small deviation from linearity of $\bar{\nu}_p(E_n)$ below 1.6 MeV has been observed.

### 3.2.4 Dynamics of fission (J. Boldeman)

A recent survey† of the kinematics of fission of the $^{240}Pu$ compound system has suggested the existence of two modes of fission. For fission above the fission barrier, the process from the saddle point to scission is adiabatic with almost all variations of the compound excitation (ignoring some minor collective effects) appearing in the excitation of the individual fragments. For sub-barrier fission, the experimental evidence suggests that the damping is zero, implying for the fully paired $^{240}Pu$ compound nucleus that the nucleons remain paired all the way to scission, consistent with superfluid motion.

One prediction of this study is that a dramatic change should occur in $\bar{\nu}_p$ at the fission barrier. Because of the considerable experimental difficulties in studying sub-barrier fission in $^{240}Pu$, we have made a preliminary investigation of this problem by performing measurements of $\bar{\nu}_p$ for below and above barrier fission of $^{230}Th$. The experimental data (Table 3.2) show that there is essentially no change in $\bar{\nu}_p$ at the fission barrier.

A possible explanation of the failure of the hypothesis in this case is the existence of the odd, unpaired neutron in the $^{231}Th$ compound system. The resolution of this question must therefore await the measurement of $\bar{\nu}_p$ for isomeric fission of an even-even nucleus.

TABLE 3.2

EXPERIMENTAL $\bar{\nu}_p$ VALUES

| Neutron Energy | $\bar{\nu}_p$ |
|---|---|
| 0.715±0.015 | 2.027±0.032 |
| 1.100±0.017 | 2.089±0.042 |
| 1.35 ±0.05 | 2.095±0.031 |
| 1.64 ±0.05 | 2.123±0.031 |
| 1.90 ±0.05 | 2.147±0.029 |

*Konchin, V. A. and Manero, F. (1972) - Atom. Energy Review, Vol. 10, 637-756
†Lachkar, J., Patin, Y. and Sigaud, J. (1975) - J. de Phys. Lettres 36, 79.

### 3.2.5 Even-odd effects in the neutron emission from $^{252}Cf$ spontaneous fission fragments (R. Walsh)

Our previous measurements of the variation of the average number of neutrons emitted per fragment as a function of the fragment mass in the spontaneous fission of $^{252}Cf$ have been repeated to confirm an apparent structure related to even-odd charge effects. In the repeated measurement, improved statistical accuracy has been obtained and a study has been made of the method of analysis of the experimental data to ensure that statistical grid effects are absent.

The previous findings have been confirmed. Fine structure in $\nu(A)$ has been observed which is consistent with that found in the fission fragment mass yields and in the variation of both the average total fission fragment kinetic energy and total $\gamma$-ray energy with fragment charge. A calculation of the even-odd charge variation of the total energy release suggests that the fine structure in $\nu(A)$ should increase with the mass of the heavy fragment. Such an increase has been observed. This effect is illustrated in Figure 3.3

## 3.3 Neutron Capture Physics

### 3.3.1 Resonance neutron capture systematics (J. R. Bird, B. J. Allen, J. W. Boldeman, M. J. Kenny, A. R. de L. Musgrove)

The increase in quality and quantity of information available on resonance parameters, particularly for medium mass nuclides and those near magic numbers, permits a new appraisal of their systematics and of the nuclear models used for their interpretation.

Of particular interest are the properties of fission products and actinides which arise as waste products in reactor systems. Many of these nuclides are unstable and cannot be measured directly. Theoretical methods are therefore required which can predict the important average resonance parameters. These methods, however, develop from a knowledge of the systematic variation of average parameters with neutron energy and mass number.

The accumulated capture and related data has therefore been examined and a review paper on this work was presented at the 1976 International Conference on Interaction of Neutrons with Nuclei, Lowell, USA.

The important parameter obtained from neutron capture reactions is the radiative width ($\Gamma_\gamma$) which gives the probability for $\gamma$-ray emission for a resonance. However, it is found that the magnitude of the radiative width can depend markedly on the angular momentum ($\ell$) of a resonance.

Average values of s- and p-wave radiative widths are plotted in Figure 3.4 as a function of mass number. The two sets of data have different structures which can be explained in terms of the dominance of E1 or M1 transitions in mass regions, which can be distinguished by the appropriate strength function maxima.

Initial state correlations (between reduced neutron widths and radiative widths or partial radiative widths) are also observed for s- and p-wave resonances in the same mass regions (Figure 3.4). The valence model of neutron capture can be used to

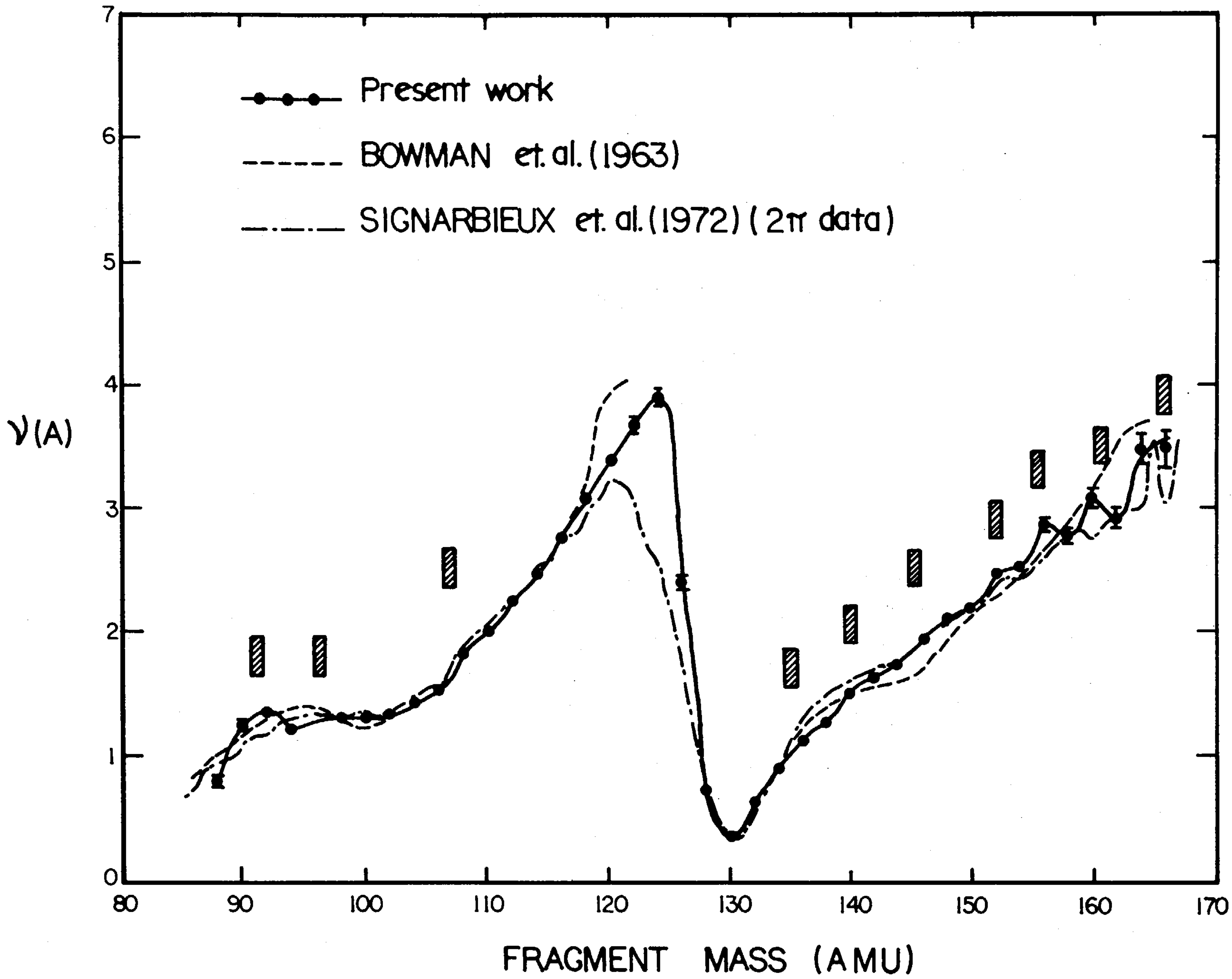


Figure 3.3 $^{252}Cf$ neutron emission as a function of fission fragment mass

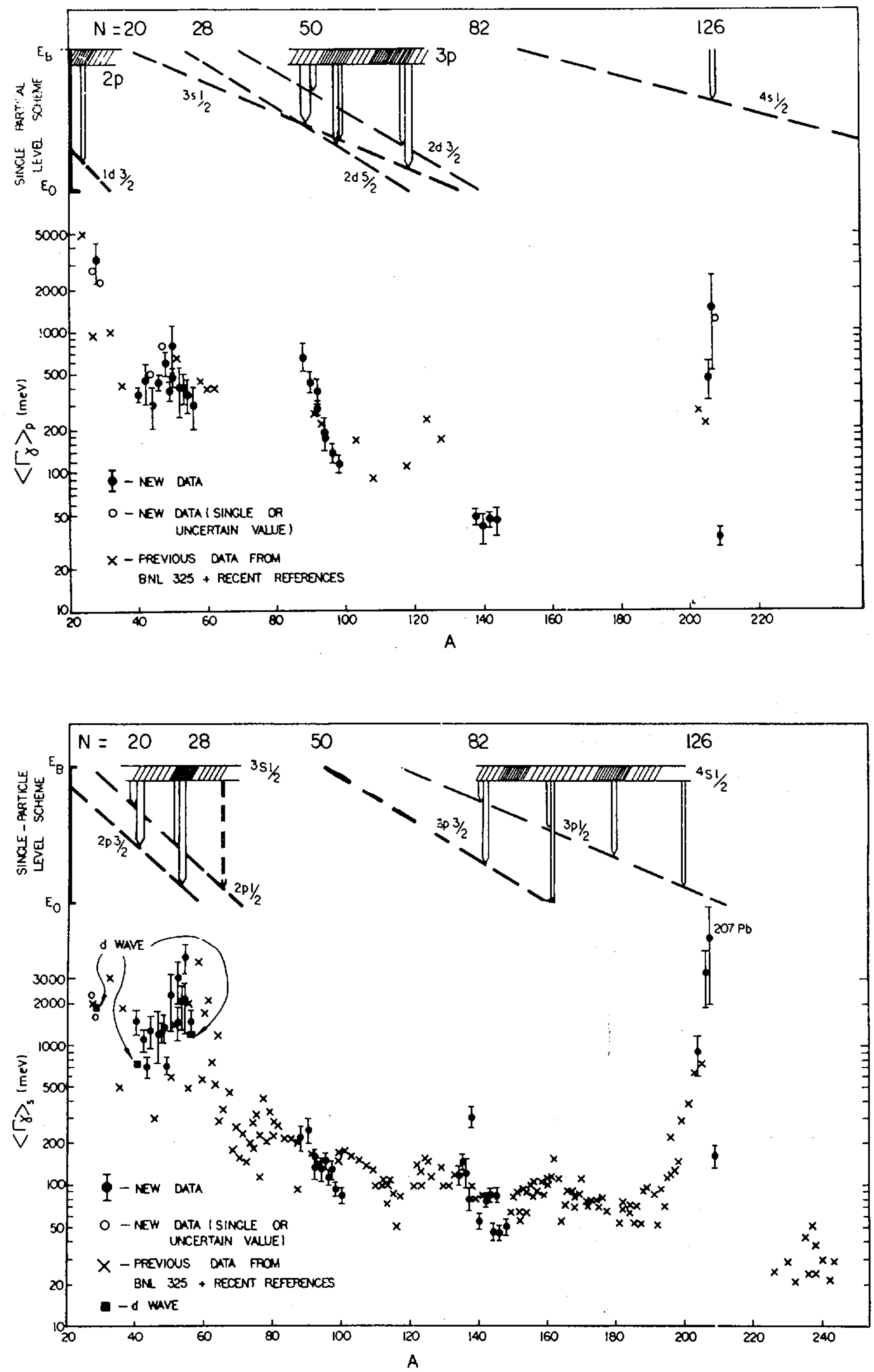


Figure 3.4 s- and p-wave radiative widths as functions of mass number

calculate the valence components of partial or total radiative widths and the ratios of calculated to observed values are included in Figure 3.5. These confirm the importance of valence capture in the 3s and 3p regions (close to N=28 and 50).

Valence capture is predicted to have negligible influence in the 4s region (for example, near N=82) and even in the 3s and 3p regions it dominates only in $^{54}Fe$ and $^{88}Sr$. Therefore, an additional capture mechanism of single particle character is required to explain the observed correlations and magnitudes of radiative widths. The excitation of 2p-1h configurations provides a satisfactory qualitative explanation of these results and calculations by various authors for specific nuclides confirms the importance of such configurations.

Additional information on the influence of single-particle states can be obtained by a study of the dependence on mass and excitation energy of strong capture $\gamma$-rays which dominate the spectra in many nuclides. These transitions follow closely the results obtained from (d,p) reactions and can be used to give additional evidence of the location of single-neutron states and the filling of neutron shells.

### 3.3.2 s-wave level spacings

The average s-wave level spacing is an important parameter in cross section calculations and also in elucidating nuclear structure, particularly near closed shells. In the course of the AAEC/ORNL capture and transmission data analyses, many new level spacings have been determined for nuclei near magic neutron numbers. From the level spacing, the level density parameter 'a' (related to the density of single particle states near the top of the Fermi sea) is calculated using the equations of Gilbert and Cameron (1965)*. The quantity a/A displays dips at magic numbers and can be correlated with shell correction energies derived from semi-empirical mass formulae. A plot of a/A versus the Cameron shell correction (Figure 3.6) shows considerable linearity despite the obsolete nature of that particular mass formula. Also shown are the Gilbert and Cameron prescriptions for deformed (lower) and undeformed (upper) nuclei.

### 3.3.3 Neutron capture cross sections (B. J. Allen, A. R. de L. Musgrove, J. W. Boldeman, M. J. Kenny)

The analysis of high resolution capture cross section data (measured at the Oak Ridge Electron Linear Accelerator by Dr. R. L. Macklin, ORNL†) has continued. Results for $^{28}Si$, $^{40,42,43,44}Ca$, $^{56}Fe$, $^{88}Sr$ and the isotopes of Zr, Mo, Ba and Nd, have been published or accepted for publication. Further papers on the Ti and Cr isotopes, $^{54}Fe$, $^{89}Y$ and $^{140}Ce$ have been submitted for publication. Work is proceeding on $^{45}Sc$, $^{57}Fe$, $^{139}La$ and the isotopes of Pb. The capture results are being incorporated in the International Nuclear Data Files for use in studies of fusion, shielding and fast reactor systems.

Some recent results and the status of current analyses follow.

---

*Gilbert, A. and Cameron, A. G. W. (1965) - Can. J. Phys. 43, 1446

†Research sponsored in part by US ERDA under contract with Union Carbide Corporation

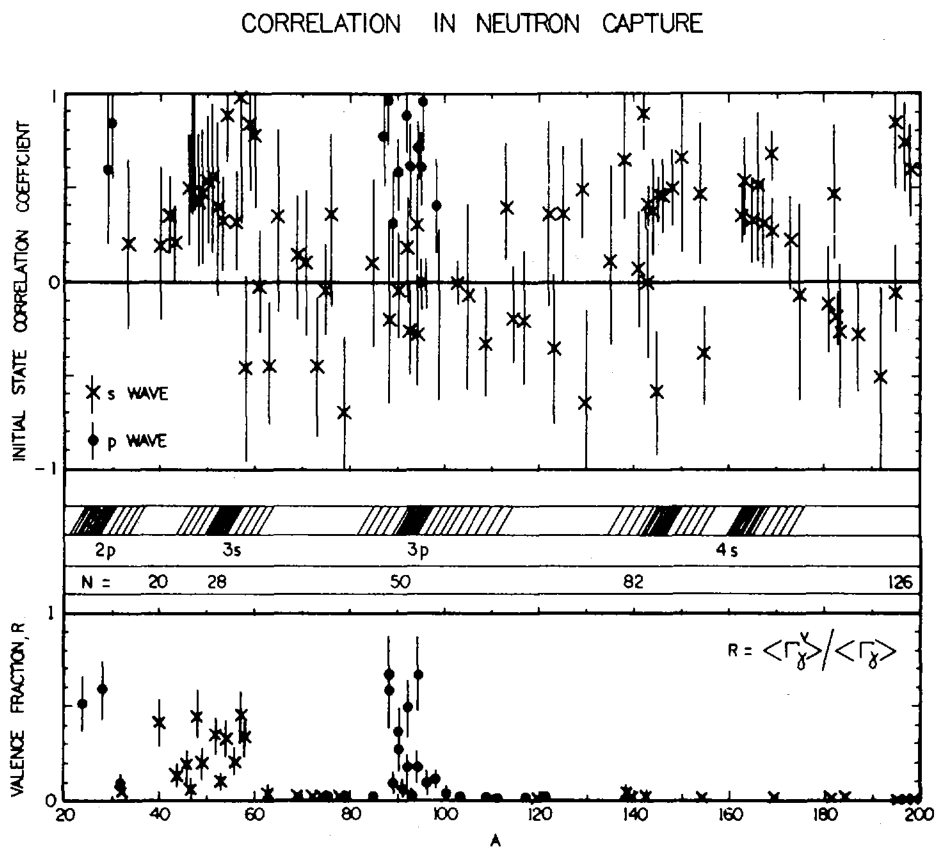


Figure 3.5 (a) Initial state correlations between reduced neutron and radiative widths

Figure 3.5 (b) Ratio of calculated to measured valence widths as function of mass number

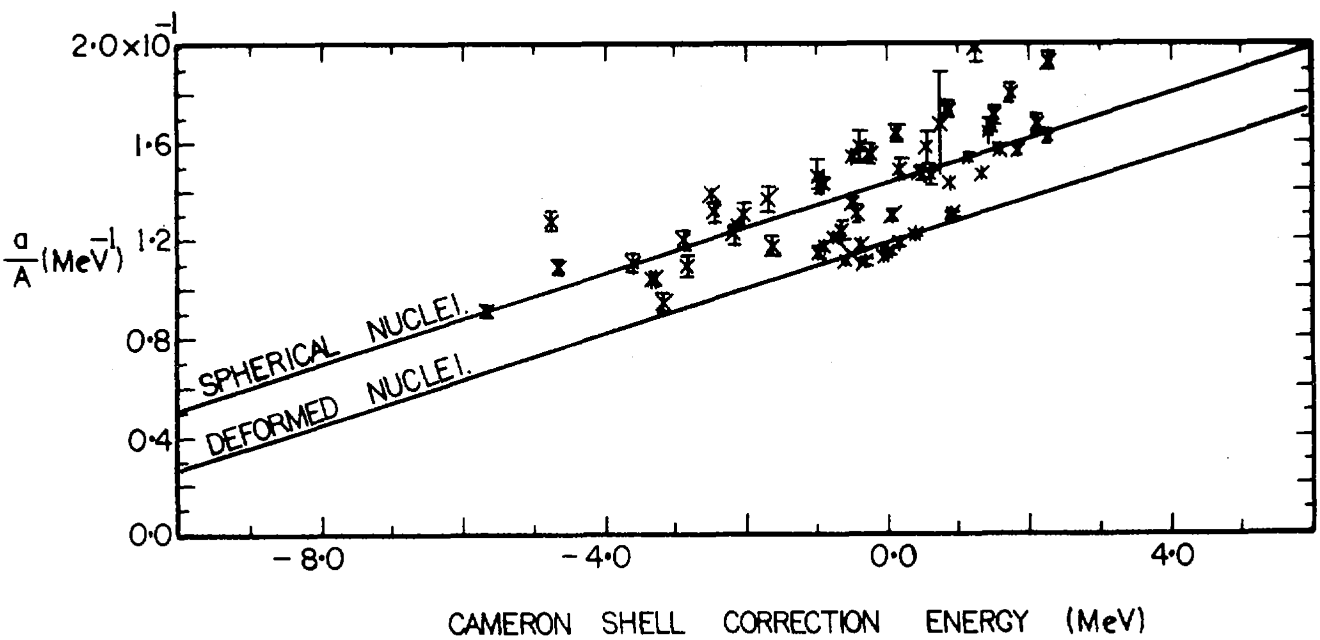


Figure 3.6 The level density per unit mass as function of Cameron shell correction

$^{23}Na$: Analysis of the capture data from 3 keV to 1 MeV has been completed. However, it is also possible to extract inelastic neutron widths up to the first excited state of $^{23}Na$ as well as the eleastic scattering widths of resonances above the threshold at 0.44 MeV. Figure 3.7 shows a plot of the capture yield excluding the 440 keV inelastic γ-ray. These data are compared with the total γ-ray yield which is dominated by the inelastic scattering component for neutron energies above 440 keV. Subtraction of the capture component permits the analysis of inelastic neutron widths for Na, which are important parameters in the neutronics of the fast breeder reactors.

$^{45}Sc$: Analysis of the capture data has been completed up to 100 keV. Accurate neutron widths of many s-wave resonances have been obtained by shape analyses, and over three times as many resonances have been observed as have previously been reported. A correlation of $\rho(\Gamma_{n0},\Gamma_\gamma) = 0.36$ is found for 27 s-wave resonances.

Ti isotopes: Substantial correlation coefficients $\rho(\Gamma_n^0,\Gamma_\gamma(s))$ have been observed for all Ti isotopes. However, for $^{48}Ti$, $\rho = 0.42$ and as this nuclide is known to decay strongly to the 2p states, a 2p-1h mechanism must be invoked to account for the low correlation. The odd isotopes also exhibit large correlations, although the valence component is relatively small. In particular, the $3^-$ resonances in $^{47}Ti$ are found to be strongly correlated ($\rho = 0.65$) while the $2^-$ resonances are not.

Cr isotopes: Normalisation of the separated isotope data has been achieved using data from a new measurement on a natural chromium target. Lower correlations are observed than have previously been reported and, again, an uncorrelated 2p-1h mechanism is required to account for the low correlation and the observed capture γ-ray spectra.

$^{54}Fe$: The valence model dominates capture only in this magic neutron nuclide in the 3s region. A correlation of 0.9 is observed and the valence model accounts for ~50 per cent of the average observed radiative widths. The s-wave data extend to 500 keV and the observed radiative widths support the predicted energy dependence of s→p valence transitions. The large single particle binding energy and s-wave strength function give rise to an average valence component, which is six times as large as in $^{56}Fe$.

$^{56}Fe$: Resonance parameter data have been extended to the inelastic scattering threshold, and inelastic widths were obtained up to 1 MeV. The s-wave data exhibit a low correlation ($\rho = 0.37$) and the valence model accounts for ~20 per cent of the average radiative widths. These results, together with γ-ray spectra up to 1 MeV, indicate the dominance of 2p-1h mechanisms in this nuclide.

$^{88}Sr$: A large correlation of 0.96 is observed for the $p_{3/2}$ wave resonances up to 400 keV, and the valence model accounts for 50 per cent of the non-statistical component, providing a quantitative verification of the valence model in the 3p region.

Zr isotopes: Significant correlations are observed in all even isotopes and, as in the 3s region, an uncorrelated component is required to fully explain the data.

Mo isotopes: The s-wave neutron strength function is close to $0.5 \times 10^{-4}$ for all isotopes, but the p-wave strength function exhibits a well defined peak near A~95.

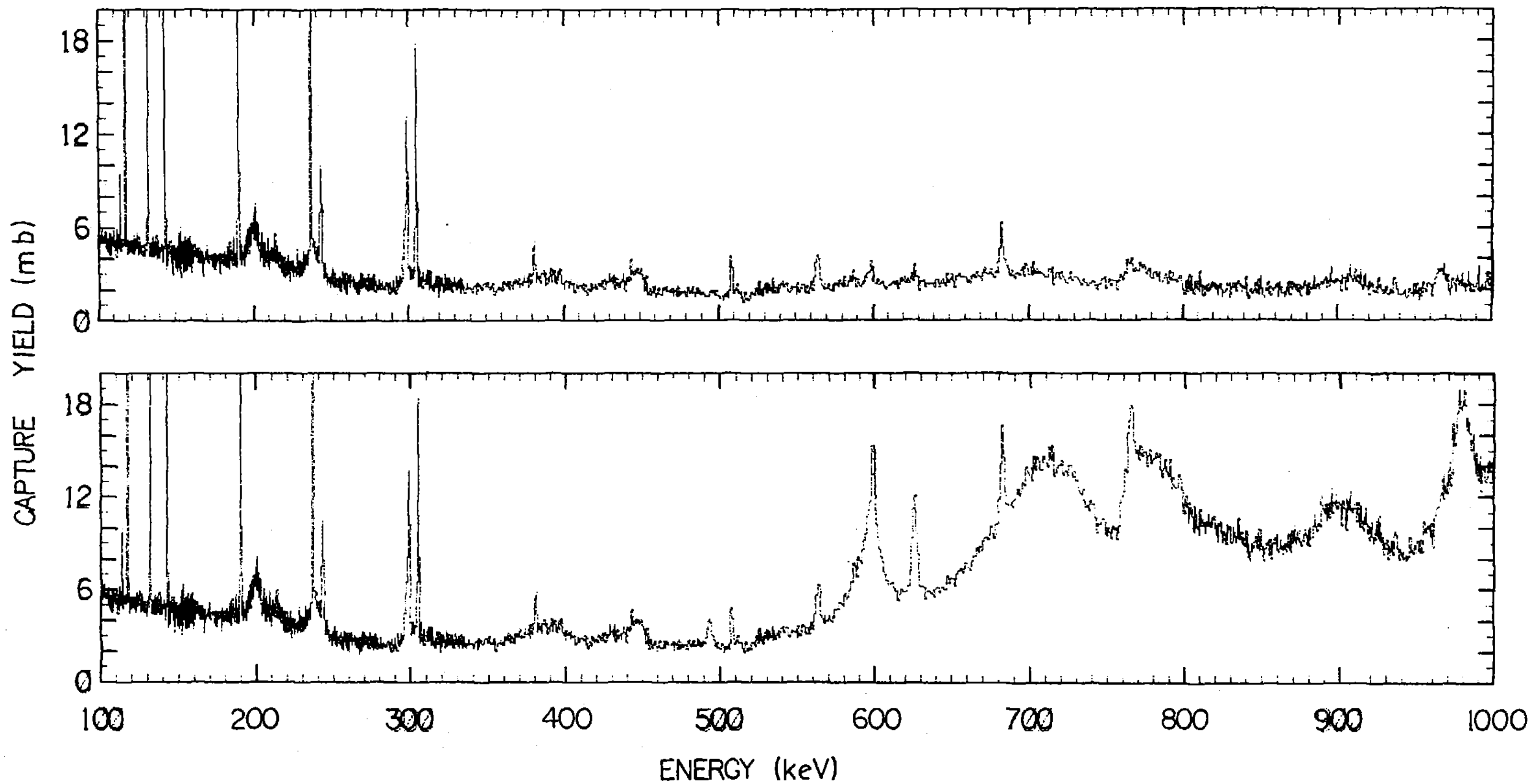


Figure 3.7 Capture yield for sodium as function of neutron energy

Both s- and p-wave radiative widths decrease markedly as further neutrons are added to the closed shell. The p-wave radiative widths are generally greater than the s-wave widths showing the presence of non-statistical $\gamma$-decay mechanisms.

Valence neutron theory fails to explain the magnitude of the difference between p- and s-wave radiative widths and doorway state processes must contribute. In particular, the data for $^{98}$Mo appear to violate the usual valence theory, since the correlations between radiative and neutron widths are small. Further, the radiative widths are smaller than can be explained on the valence model. An explanation for the loss of valence strength has been advanced.

Interpolated resonance parameters allow an estimate to be made for the unknown cross section for $^{99}$Mo(n,$\gamma$).

Nd isotopes: Significant positive correlations were found between $\Gamma_n^0$ and $\Gamma_\gamma$ for all isotopes. The magnitude of the observed correlation coefficient, particularly for $^{142}$Nd ($\rho$ = 0.9), cannot be explained in terms of valence neutron capture and an additional mechanism is required.

The average s-wave radiative widths for the odd-A isotopes were found to be markedly greater than for the even-A isotopes while the p-wave radiative width for Nd was considerably less than the s-wave width.

$^{140}$Ce: As in the N=82 nuclides ($^{138}$Ba, $^{142}$Nd), a significant correlation is observed ($\rho$ = 0.6) which cannot be accounted for by the valence model.

### 3.3.4 Total cross sections

Correlations between the reduced neutron widths and radiative widths are frequently observed. Analysis of the correlations require neutron scattering widths ($\Gamma_{\lambda n}$) with high accuracy. Scattering data are being obtained from ORNL which complement the capture results and lead to improved resonance parameter sets.

Transmission data taken (by J. A. Harvey, ORNL) at 80 m and 200 m stations of ORELA have been analysed using a non-linear least squares fitting routine. The data for $^{92,94}$Zr were analysed in conjunction with the (n,$\gamma$) data from the 40 m station and resulted in an almost complete set of resonance parameters for these two isotopes to abofe 100 keV.

A similar analysis of 200 m data on $^{90}$Zr has given parameters for resonances up to 300 keV. Several assignments reported from threshold photoneutron measurements ($^{91}$Zr($\gamma$,n)) by Toohey and Jackson (1974)* were found to be incorrect. In particular, the 119.8 keV resonance was reported as g=2, but our shape analysis (Figure 3.8) clearly indicates that this is a $p_{1/2}$ resonance. The average s-wave parameters obtained for $^{90}$Zr are as follows: $\langle D \rangle$ = 8.6±1.6 keV, $S_0$ = (0.54±0.14) x $10^{-4}$. For the two p-wave sequences, the following average parameters were obtained: ($p_{1/2}$) $\langle D \rangle$ = 8.6±1.6 keV, $S_1$ = (3.9±1.0) x $10^{-4}$; ($p_{3/2}$) $\langle D \rangle$ = 4.3±0.8 keV, $S_1$ = (4.3±0.8) x $10^{-4}$.

The analysis of the 80 m data on $^{91}$Zr (an important fission product) is well advanced, and a portion of the data is given in Figure 3.9. The analysis above

*Toohey, R. E. and Jackson, H. E. (1974) - Phys. Rev. C9, 346.

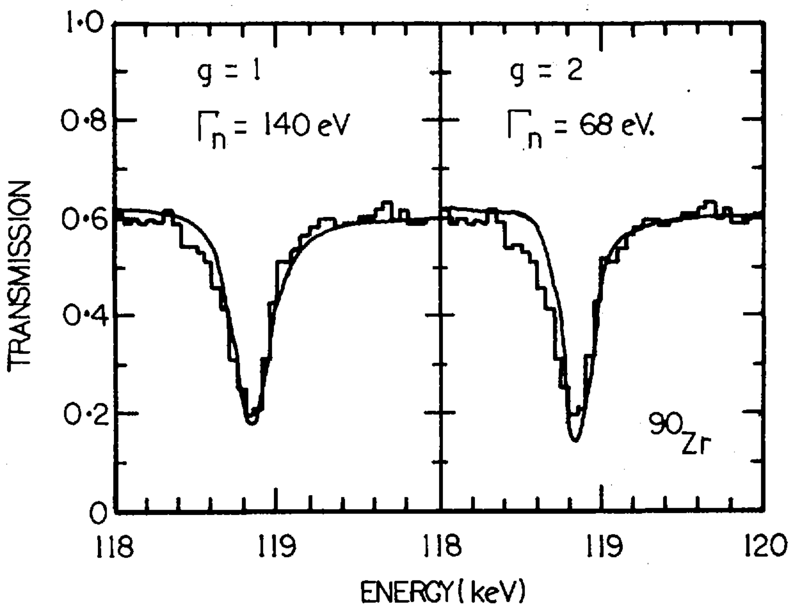


Figure 3.8 Fits to the 118.8 keV resonance in $^{90}Zr$ assuming g=1 and g=2 respectively

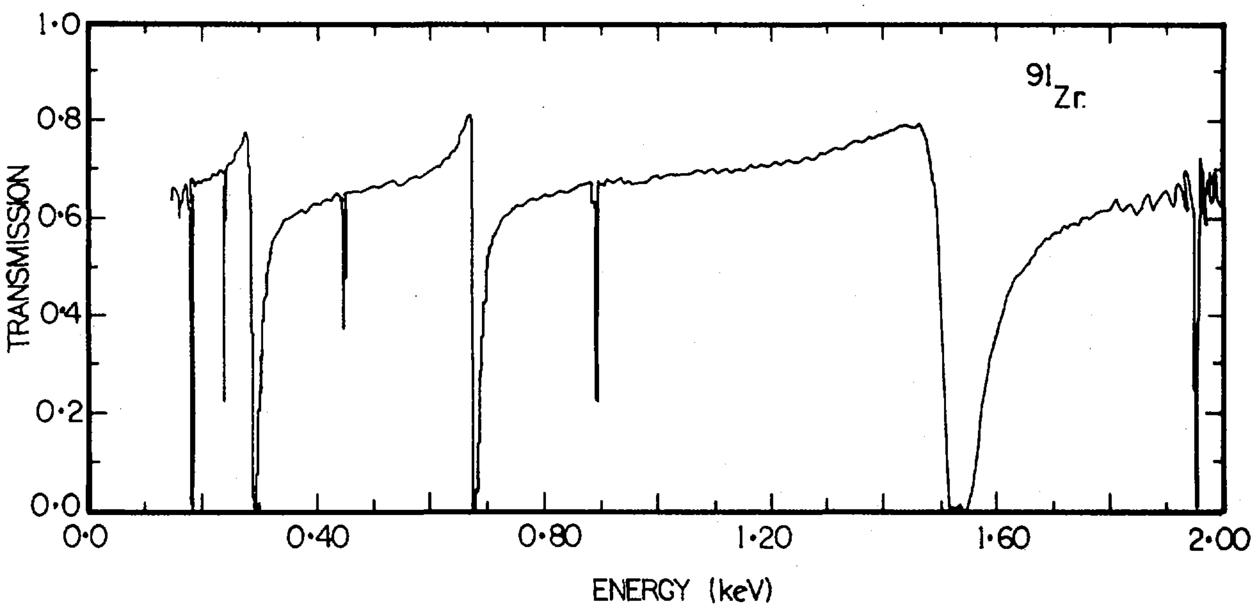


Figure 3.9 Neutron transmission data for $^{91}Zr$ taken at 80 m station, ORELA

3 keV is proceeding in parallel with a re-analysis of the (n,$\gamma$) data (reported in AAEC/E367 1976) and it is anticipated that resonance parameters up to 100 keV will be obtained using the 200 m run.

### 3.3.5 Partial capture cross sections of $^{91}$Zr, $^{111,113}$Cd, $^{117,119}$Sn

Nuclides in the 3p mass region exhibit correlations between the p-wave reduced neutron widths and radiative widths and total cross section data has shown evidence for intermediate structure. The valence model has had only limited success in accounting for experimental data and a qualitative interpretation in terms of a 2p-1h interaction has been given.

In a search for the possible occurrence for intermediate structure, measurements have been made on odd-A nuclides in the 3p region. A Ge(Li) detector was used to observe averaged $\gamma$-ray intensities from capture of 10-80 keV neutrons by $^{91}$Zr, $^{111,113}$Cd and $^{117,119}$Sn. The results were converted to absolute partial cross sections using the 35 keV resonance in aluminium for normalisation.

For the cadmium isotopes, the smooth energy dependence of the observed partial capture cross section (Figure 3.10) is similar to the estimated elemental p-wave cross section. Transitions to the ground and first excited state account for 10 per cent of this cross section and valence model calculations account for only 25 per cent of the observed strength. No evidence was seen for intermediate structure in the 10-80 keV energy range.

In tin, some evidence was found for intermediate structure above 60 keV, but confirmation is required. The zirconium data provided only limited information because of the low cross section of $^{91}$Zr.

### 3.3.6 Non-statistical effects in neutron capture (0.04-1.00 MeV)

The survey of capture gamma ray spectra for neutron energies up to 1 MeV has been concluded. Marked non-statistical effects were found in the spectra from elements in the mass regions where the 3s, 3p and 4s neutron strength functions maximise. Figure 3.11 shows unfolded NaI spectra for 3s region nuclei (Ca, Ti, Cr, Fe, Ni and Zn) at a number of neutron energies. The non-statistical nature of these spectra is clearly seen.

Results for the 3s and 3p regions frequently show enhanced transition strengths to final states with a strong single particle nature. Even though the valence model should be applicable for these nuclei, calculations show that, in general, valence capture alone is unable to account for all of the enhanced strength.

In the calcium data of Figure 3.11, transitions to the $^{7}/_{2}^{-}$ ground state of $^{41}$Ca are observed. New calculations for d-wave valence capture predict greater strengths than are observed at low neutron energies, but give reasonable agreement above 200 keV. The disagreement at low energies may point to depletion of the d-wave

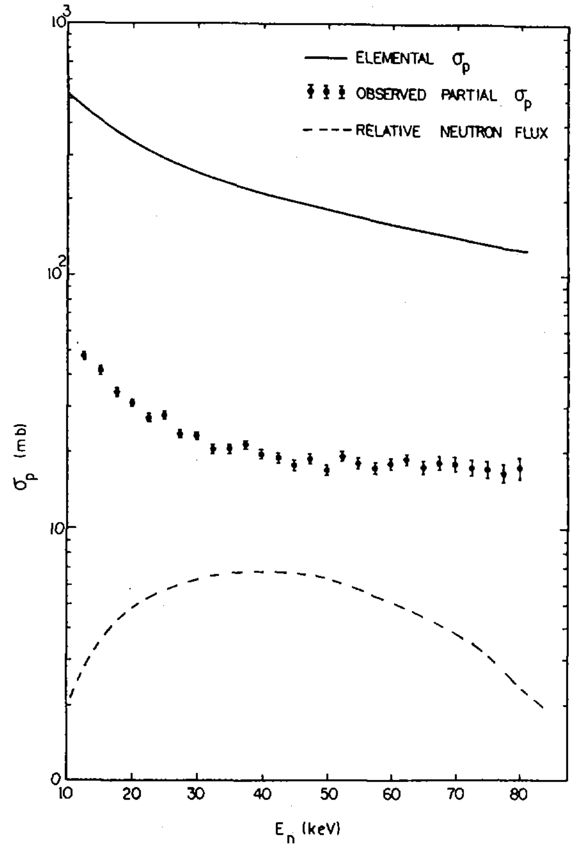


Figure 3.10 Cadmium partial capture cross sections obtained from measured neutron capture γ-ray intensity

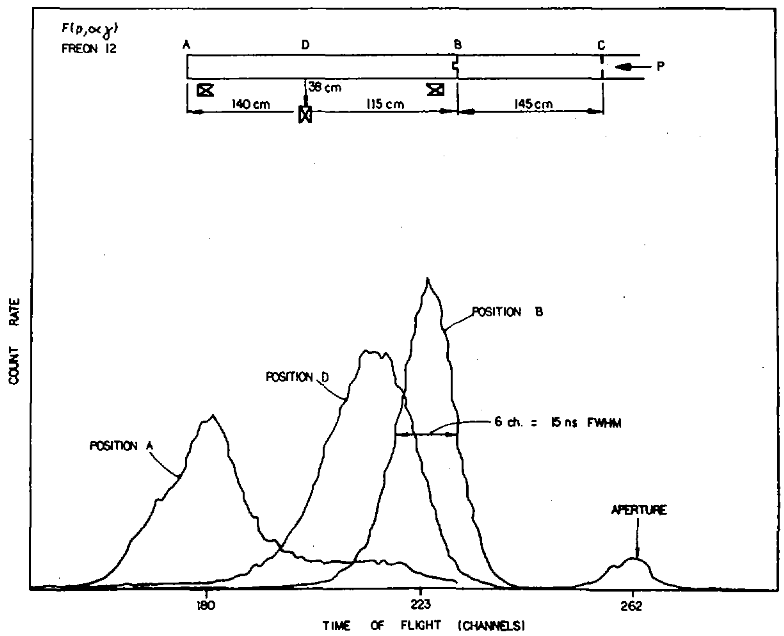


Figure 3.13 Time of flight spectra for the F(p,αγ) reaction are shown for various detector positions

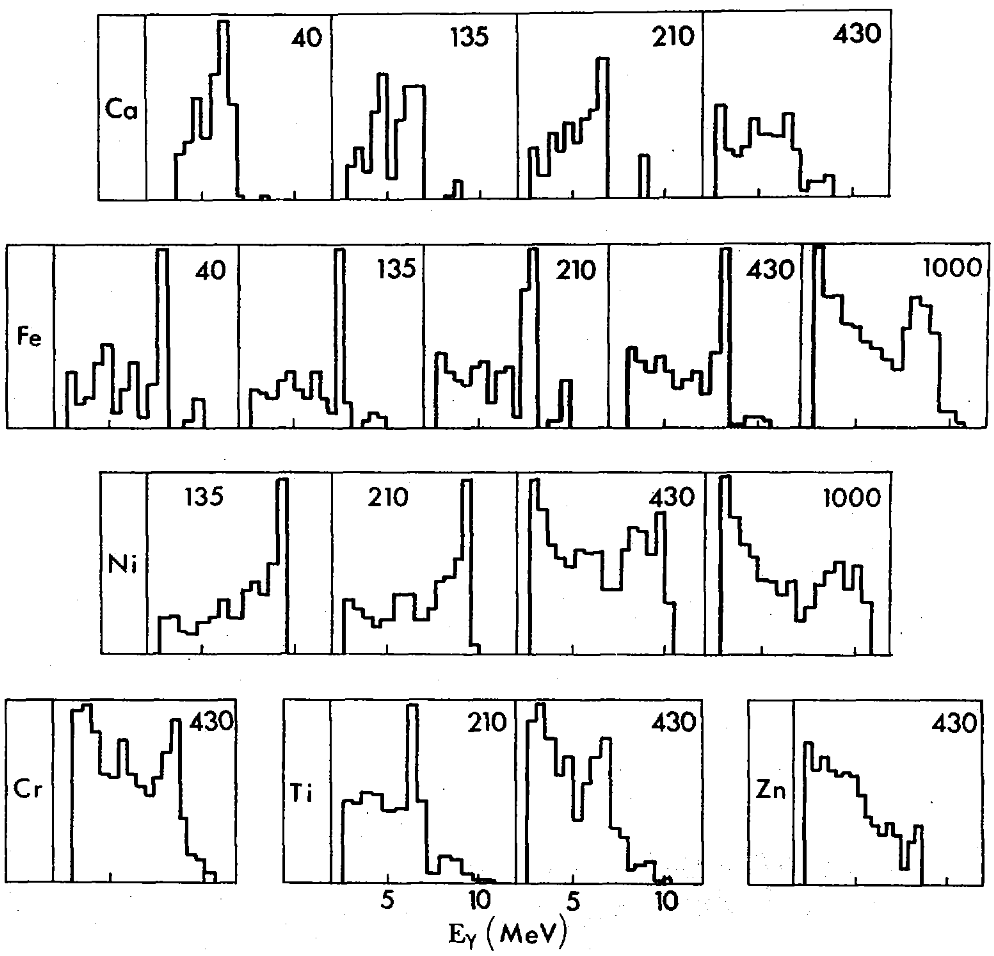


Figure 3.11 Unfolded spectra from 3d nuclei at various energies

dipole strength, but fluctuations in d-wave resonance spacings and neutron widths qualify this interpretation. Since the valence model can adequately account for the d-wave dipole strength abofe 200 keV, it is concluded that there is no significant depletion (by the giant resonance) for the $^{40}Ca(n,\gamma)^{41}Ca$ reaction above 200 keV.

### 3.3.7 Neutron flux measurements

Absolute partial capture cross sections require a knowledge of the neutron flux. A thin $^{6}Li$ glass detector has been calibrated in the energy range 10-220 keV. Yields from the $^{7}Li(p,n)^{7}Be$ reaction at a number of neutron energies agree with predicted values to within 10 per cent.

A manually rotatable lithium target was developed so that fall off in flux, due to target deterioration under bombardment, could be eliminated.

## 3.4 Prompt Nuclear Analysis (J. R. Bird, L. H. Russell, M. D. Scott, A. van Heugten, B. J. Allen, M. J. Kenny, H. Broe)

### Characterisation of Obsidian

Following the successful use of proton induced gamma rays to obtain rapid characterisation of obsidian samples from known source locations, an improved experimental system has been used for the study of approximately 500 artefacts from the South West Pacific (in collaboration with W. Ambrose, School of Pacific Studies, Australian National University).

A Ge(Li) detector with 21 per cent relative efficiency was used, without any X-ray filter, to give 5-10 x $10^{4}$ counts in the 440 keV peak from Na gamma rays with a 3-5 min irradiation by a 200 nA proton beam. Spectrum stabilisation, sample positioning and peak area analysis are carried out by the PDP-15 computer system so that up to 50 samples can be run in an unattended sequence. Areas of gamma ray peaks from F, Na and Al in the sample, ratios of peak areas and other parameters used to check performance, are printed out at the end of each run.

Measurements were also made of the experimental factors affecting the accuracy of the observed results and of the standard deviation of measurements made at different positions on samples from one source. Data taken under constant experimental conditions were also used to compare observed peak areas from three elements, and this gives better differentiation between some sources which have similar values for peak ratios.

The surface condition of the artefacts varied greatly, but satisfactory allocation to source locations was possilbe from the first run on all but 5 per cent of the samples. Repeated runs provided satisfactory results for the remaining samples. The results showed the presence of a group of artefacts from a location not identified in the known source samples.

### Analysis of Glass

The quantity of sodium in commerical glass has an important influence on its behaviour during production processes. The measurement of prompt gamma rays from proton irradiation has been used to obtain the level of sodium in samples of bottle glass with a standard deviation of 1.6 per cent (for 13 per cent soda, Table 3.3).

Using the same experimental system as for obsidian analysis, measurements can be made in 3-5 min so that, although specialised equipment is required, this technique is competitive with chemical analysis. Routine measurements are planned under contract to Australian Consolidated Industries.

During the measurement of sodium, additional spectrum peaks give information on B, F and Al. The results for fluorine are of particular interest in the study of the treatment of bottles with organic fluorides to prevent 'bloom'. Tests have also been carried out (in collaboration with D. G. Owen and B. Coniglio, A.C.I) on the use of proton backscattering to determine the thickness of tin oxide layers following treatment of hot glass with stannic chloride.

TABLE 3.3

SODIUM CONTENT OF GLASS

| Sample | Counts in 440 keV Peak | | | | |
|---|---|---|---|---|---|
| 1 | 110247 | 109969 | 111900 | 108581 | 110537 |
| 2 | 108517 | 106770 | 110780 | 107003 | 109516 |
| 3 | 111409 | 111520 | 111243 | 110096 | 111335 |
| 4 | 110847 | 109664 | 112616 | 110510 | 110598 |
| 5 | 108940 | 109537 | 108811 | 108067 | 109343 |
| 6 | 110656 | 109472 | 108144 | 112999 | 112009 |

Mean = 110043. Standard deviation = 1606 (1.6%)

## Gettering by Silica

The presence of aluminium on the surface of silica, used to getter molten germanium, has been studied using (p,p') and (p,$\gamma$) reactions. Observation of the 992 keV resonance in the latter reaction shows a shift of 1.5 keV, which is caused by charging of the insulating sample, The amount of aluminium present is determined by comparison with evaporated layers.

## Solar Absorber Surfaces

Measurements have been made on wavelength selective solar energy absorbers (provided by School of Physics and Materials, New South Wales Institute of Technology), consisting of chromium black on copper. Backscattering techniques give information on the thickness of the surface layer, as well as the amounts of oxygen and chromium present. The oxygen content can also be studied using the $^{18}O(p,\alpha)$ reaction, while the chromium component can be determined using the $^{52}Cr(p,p'\gamma)$ reaction. These techniques are particularly suitable for the study of layers up to several microns thick.

## Ancient Bronze

Preliminary tests have been carried out of the usefulness of backscattering and prompt gamma ray techniques for the non-destructive analysis of the surface of ancient bronze artefacts (provided by N. Barnard, School of Pacific Studies, Australian National University). Information can be obtained in this way on:

(a) the composition of inlay, joint and host materials,

(b) the composition of corrosion products, and

(c) materials used in specialised surface treatments.

Results show major variations between samples and between positions on individual samples (Figure 3.12), but further measurements are needed to clairfy the usefulness of this information.

## External Beam

A 2.5 μm thick nickel window at the end of the accelerator beam line has been used to allow a proton beam to pass through and irradiate large samples located outside the accelerator vacuum system. A very simple analysis system is then possible with a gamma ray detector placed behind the sample, but corrections must be made for attenuation of the gamma rays in passing through the sample thickness.

## Thorium Analysis

Samples containing thin layers of powdered thorium ores have been prepared in order to compare the results of proton induced X-ray analysis with those of delayed neutron techniques. Preliminary X-ray measurements (carried out by C. S. Newton, Australian National University and G. J. Clark, CSIRO) verified that a thorium concentration of 100 ppm can be readily observed.

## Fluorine in Gases

The detection of high energy gamma rays from the $^{19}F(p,\alpha\gamma)$ reaction can be used to detect gaseous fluorine compounds at pressures down to $10^{-3}$ torr. The spatial distribution of fluorine has been studied by using a pulsed proton beam and measuring the time dependence of gamma ray yield using a NaI detector (Figure 3.13). The time of flight of the protons through the gas and their rate of energy loss must be unfolded from the time spectrum to obtain the spatial distribution. An alternative method used the active isotope $^{20}F$ produced by deuteron irradiation.

## Bibliography

The summary and bibliography of published reports on Prompt Nuclear Analysis Techniques, which was published in 1974* has been updated to include publications up to the end of 1975. The literature on this topic has doubled in 2½ years, showing a rapid acceptance of these techniques in some fields and a growing effort in the development and demonstration of new applications.

---

*Atomic Energy Review 12 (1974) 275

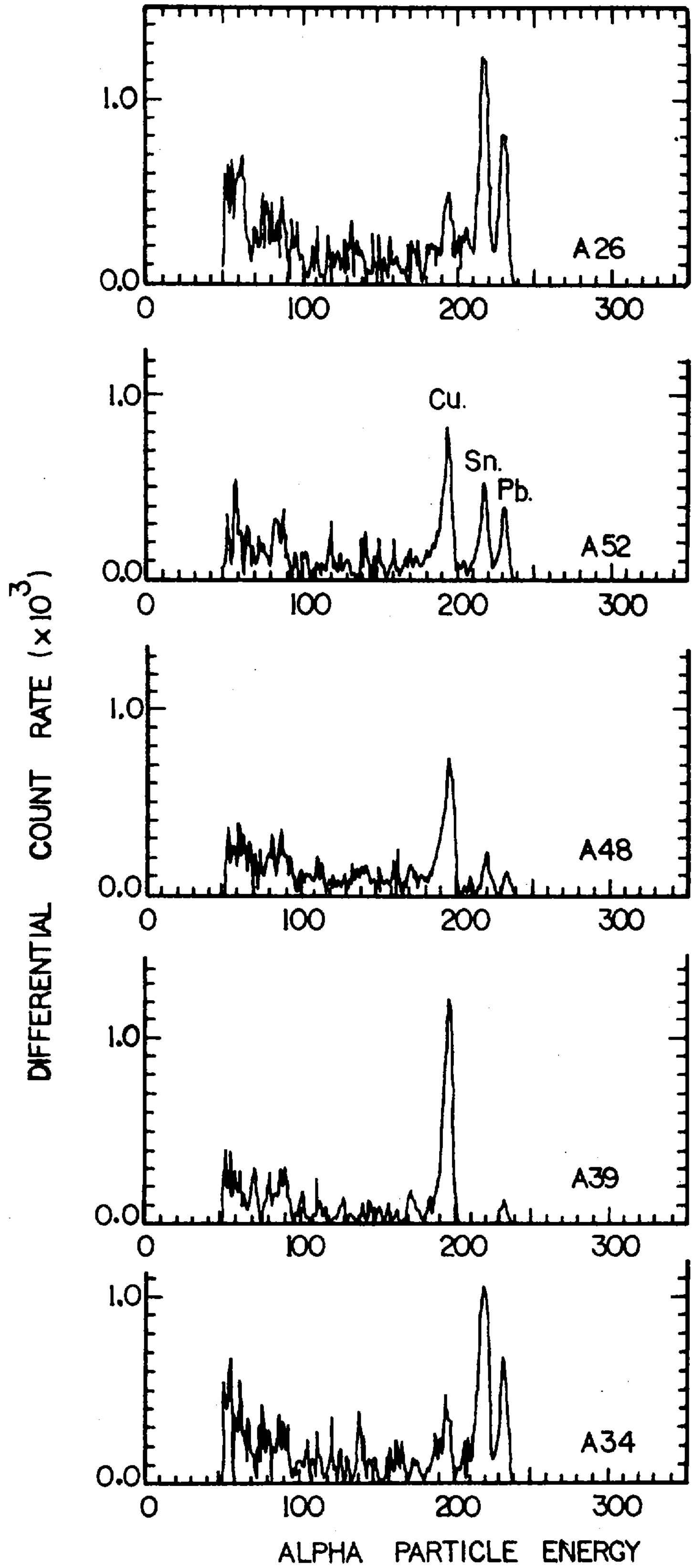


Figure 3.12 Differentiated gamma spectra obtained from gammas scattered from ancient bronze specimen

# 4. THEORETICAL PHYSICS

## 4.1 AUS Modular Scheme (B. E. Clancy, B. Harrington, J. Pollard, G. Robinson)

The AUS suite of modules used for reactor calculations has been subjected to detailed checkout during the period. A number of minor revisions were made.

### 4.1.1 AUS module EDIT (J. Pollard)

The new EDIT module has been written and tested and is now in regular use. The basic function of EDIT is the routine editing of group fluxes produced by diffusion and transport modules to give neutron reaction rates with the material cross sections supplied to these modules. These - typically few group - cross sections will have been generated by other modules of the system by mixing different nuclides and by group collapsing over various five group spectra. The history of this smearing and group collapsing is available in the STATUS data pool and the EDIT module also has the function of 'unscrambling' this history to provide total of five group reaction rates for any nuclide in the mixed material.

Input data preparation for the module is simplified by adhering to the AUS data philosophy of providing sensible default values for most input items.

### 4.1.2 AUS module MIRANDA (G. Robinson)

Some difficulties have been experienced with the fitting of group resonance integrals with subgroup parameters and their subsequent use in MIRANDA. The initial work in this area was performed for $^{238}U$ data prepared by the British GENEX code, which did not include interference scattering. The $\lambda$ method required some modification when interference scattering is included. The modification has been made and the calculated results are now acceptable.

A further difficulty was experienced in obtaining an accurate representation of resonance overlap when interference scattering was involved. This problem was overcome by including, with the subgroup parameters in the cross section library, additional factors for the group flux depression.

In the calculation of overlap-corrected resonance integrals, the group flux depression is used to generate a pseudo resonance cross section which is included with the potential scattering correction.

### 4.1.3 AUS.ENDF/B cross section library (B. Harrington)

Preparation of AUS cross section data from ENDF/B-IV data files has continued. During the year ENDF/B-IV data for the following nuclides has become available on the standard AUS.ENDF/B library: $^{234}U$, $^{236}U$, $^{164}Dy$, $^{176}Lu$, $^{115}In$, Rh, $^{63}Cu$, $^{56}Fe$, Au.

## 4.2 Radiation Shielding

### 4.2.1 Shielding codes (I. J. Donnelly, B. J. McGregor)

The RSIC data library, DLC-27, a 126-group coupled neutron and $\gamma$-ray cross section set, has replaced DLC-9 (AAEC/PR40-P, section 4.3).

The code APRFX-I is used to condense multigroup cross sections to a coarser group structure using either an input flux spectrum or a calculated diffusion theory flux spectrum. It has been modified to handle coupled neutron and $\gamma$-ray cross section sets and to produce output on disk in a form suitable for the transport code ANISN. It is now a convenient link between cross section libraries such as DLC-27 and ANISN.

4.2.2 Modified diffusion theory for neutron shielding (I, J. Donnelly)

The diffusion approximation for neutron transport is expected to be inadequate near boundaries of dissimilar media and in media with large absorption. In many neutron shields the latter drawback is the principal determinant of the accuracy of diffusion theory for prediction of the high energy neutron flux. An attempt has been made to improve the accuracy of diffusion theory for shielding calculations by allowing the diffusion coefficient to vary in order to compensate for the effect of large absorption. One promising method, which has been analysed in one dimension, is to define a flux dependent diffusion coefficient of the form:

$$D(K) = \left[\tanh^{-1}(K)-K\right]/\left[\sigma_{tr}K^2\tanh^{-1}(K)\right] \qquad \ldots(1)$$

where $$K(x) = (d^2\phi/dx^2)/\phi \qquad \ldots(2)$$

The diffusion equation then becomes:

$$-\frac{d}{dx}\, D(K)\, \frac{d\phi}{dx} + \sigma_a\phi = S \qquad \ldots(3)$$

This expression for the diffusion coefficient has been derived from asymptotic transport theory. It reduces to the standard diffusion coefficient for K small. Equation (3) is non-linear and must be solved iteratively.

A one-dimensional, multigroup, finite difference code has been written and the method applied to several test problems, with mixed results. If the usual three point finite difference expression for $d^2\phi/dx^2$ is used to evaluate K in equation (2), the converged solution sometimes contains non-physical oscillations. This fault can be avoided by using equation (3) to obtain an approximate value for $d^2\phi/dx^2$, and hence for K. In the test problems which were designed to resemble thick, homogeneous shields, the method predicted accurate fluxes, even for large absorption. However, flux discontinuities were found to occur at material interfaces with a consequent loss of accuracy. Several modifications are being tried in an attempt to overcome this problem.

An extension of the method to two dimensions is not straightforward because of the directional dependence of the modified diffusion coefficient. It is thought that a finite element formulation of the problem has the best chance of success; however, this is first to be tested in one dimension to ascertain whether the method is stable.

One of the advantages of the finite element method is that for small element size, h, the solution can be predicted to converge as $O(h^p)$ where p depends on the basis functions used and on the differentiability of the solution. In order to obtain some insight into the relative merits of the most commonly used basis functions, and to analyse the behaviour of the finite element solution for large as well as small elements, the finite element form of the one-dimensional, one-group diffusion theory equation has been solved analytically for a few simple test problems. Linear, quadratic Lagrangian, cubic Hermite and cubic B-spline basis functions were used. In each case, the expected convergence of the flux was obtained for small h. For larger h, it was found that oscillatory behaviour of the nodal fluxes can occur, particularly for linear and cubic spline basis functions.

4.2.3 Gamma ray spectrum from ores (B. J. McGregor)

The influence of overburden on $\gamma$-ray spectrum from deeply buried ore bodies has received further study. A method has been developed for representing the energy dependent response of the NaI detector. A second experiment was designed to overcome deficiencies revealed by the first CSIRO experiment. Analysis of this experiment revealed inconsistencies both internally and with respect to the previous experiment.

Based on this work, a new experiment with improved instrumentation was undertaken. Analysis of this experiment gave good agreement between calculation and experiment. The outcome of this initial work is that regions of the energy spectrum (windows) exist which characterise or indicate the depths of overburden between the ore and detector. The usefulness of the method in the field on an actual ore body has yet to be demonstrated.

4.3 Proton Recoil Liquid Scintillator Neutron Spectrometers
(S. Whittlestone, E. Clayton)

Development of small neutron spectrometers based on the liquid scintillator NE213 has continued. Replacement of the perspex light guides by quartz had led to an increase in light transmission from 25 to 80 per cent. A further factor of 1.3 increase in the light reaching the photomultiplier has been achieved by using a conical rather than a cylindrical scintillation chamber. The chamber itself is now made of quartz rather than perspex to improve the optics of the system, and to reduce the perturbing effect of the detector on assemblies into which it is inserted.

As part of a program to determine the efficiency and response functions of these small detectors, the efficiency of a relatively large NE213 scintillation chamber (50 mm diameter x 36 mm thick) was determined for neutrons with energies in the range 0.1 to 10 MeV. From 2 to 4 MeV the absolute efficiency was measured using an associated particle rig developed at the Australian National University and Lucas Heights by an AINSE Research Fellow. The efficiency between 1 and 10 MeV was calculated using a code developed at Lucas Heights, and the results normalised (4 per cent adjustment) to the associated particle measurements. As a final step, the detector efficiency relative to a long counter was measured in the range 0.1 to 1.2 MeV and normalised at 1.2 MeV to the 1-10 MeV data.

A further measurement of this detector efficiency and that of the smaller detectors will be carried out at ANU using the associated particle rig, using the wider range of neutron energies available from the ANU accelerators.

The Monte Carlo code described in previous reports, has been modified to incorporate the variation of light collection efficiency over the detector. It is assumed that the light collection efficiency (the number of photons arriving at the photomultiplier after an event) can be modelled by a Gaussian distribution of mean $\mu_L$ and variance $\sigma_L^2$. These parameters are measured. The photomultiplier resolution function, $R(y,y')$, describes the probability of an output pulse height $y'$ occurring given an input pulse height y, and this function tends to be a Gaussian in y' when y is large. Given that both the light collection and photomultiplier resolution functions approximate Gaussians, their combined resolution function will have a variance obtained by adding the individual variances, thus:

$$\sigma^2 = \sigma_L^2 + \sigma_{PM}^2$$

where $\sigma_{PM}^2$ is the variance of the photomultiplier resolution function. With this definition of $\sigma^2$, the original form of the photomultiplier resolution function R can be retained if the pulse heights y,y' are modified to

$$Y = 2y/(2+c^2y) \quad ,$$

$$Y' = 2y'/(2+c^2y') \quad ,$$

with

$$c = \sigma_L/\mu_L \quad .$$

In the present applications, c may be as high as 0.11.

## 4.4 Reactor Data

### 4.4.1 Fission product cross section library (J. L. Cook, H. D. Ferguson, E.K. Rose)

Since the 192 nuclide fission product cross section library was prepared in 1972, much new information has become available for more than the initial 33 elements used. There are now some resolved resonance data for 20 nuclides where none previously existed. Level spacings and strength functions have been determined for about 15 more nuclides. We therefore proposed to re-determine cross sections for the 192 nuclide set, but leaving out the 78 nuclides treated in the ENDF/B-IV library. Work has begun on a re-determination of the theoretical parameters which allow us to extrapolate level spacings to nuclides where no measurements have been made. A compilation has been made of some 200 measured level spacings covering the whole periodic table.

A Monte Carlo program has been written to calculate cross sections of elements whose thermal capture cross section values and resonance integrals have been measured. The error distribution in the cross sections computed was investigated and found to approximate to a normal distribution. The program produces point cross sections in the ENDF/B format. Initially, we proposed to deal only with those nuclides where just the thermal cross section and resonance integral have been measured. There are about 115 of these, mostly unstable but long-lived. The statistical region of some of these cross sections can be checked as about 40 values for the 30 keV cross section have been measured.

### 4.4.2 Resonance parameter analysis (J. L. Cook, E. K. Rose)

There exists a discrepancy concerning the number of channels open in the $J=4^+$ state of $^{235}U$. Analyses of the low energy resonances, where spin assignments have been made, indicate that there are approximately three channels open. However, a theoretical analysis of the fission cross section in the keV range using the double-humped fission barrier type of potential indicates that only one channel is appreciably open. It was suggested that the low energy data could be in error if many small fission widths were missed as the result of the multilevel analysis. We tested this hypothesis.

The statistical distribution of fission widths for one open channel was evaluated in groups containing roughly equal numbers of levels. The groups with smallest widths were gradually reduced in the number of widths and the resultant distribution refitted with the more general fission width distribution that is a function of the number of open channels. It was found that even if all fission widths were missing, the effective number of open channels, though increased, only reached a value of 2.6.

In this way, a distribution that is in reality that for one open channel, can appear to arise from a distribution with 2.6 open channels, solely because of missing levels. Owing to the extremeness of this situation, we were forced to conclude that the above discrepancy could not be explained by the missing of small fission widths in the resonance parameter analysis.

4.4.3 Statistical theory (W. K. Bertram)

The original Hauser-Feshbach theory has been widely used for the evaluation of average reaction cross sections. Notwithstanding its apparent success, it has long been realised that it is based on rather restrictive conditions which are not satisfied in many of the reactions to which the Hauser-Feshbach theory has been applied. Early attempts to formulate a statistical theory on a more mathematically vigorous basis resulted in Moldauer's statistical theory. However, Moldauer's theory contained inconsistencies which rendered it unsuitable for the evaluation of cross sections. A later Hauser-Feshbach formula has been proposed, based on empirical results obtained from the results of computer experiments.

Therefore, a more general statistical theory has been derived from the properties of unitarity and analyticity of the S matrix. These investigations resulted in a formal theory in which the Hauser-Feshbach theory and its more recent derivative, appear as special cases. Although our formalism obviates the difficulties and inconsistencies encountered in Moldauer's theory, its application to the evaluation of certain cross sections still presents problems, investigations into which are still being carried out.

4.4.4 Reactor calculations and nuclear information (D. Lang)

The nuclear parameters used in reactor calculations are constantly being revised as experiments become more accurate. The reactor calculations accordingly need to be kept up to date. From time to time, it is suggested that the process shoudl work both ways, and that a comparison of nuclear reactor constants as determined by experiment and calculation should lead to revision and improvement of the nuclear data that comes initially from microscopic experiments. A study of the formalism developed by Usachev and Bobkov* has been made. The formalism has been found to be

---

*Usachev, L. N. and Bobkov, Yu. G. (1972) - Planning an optimum set of microscopic experiments and evaluations to obtain a given accuracy in reactor parameter calculations. INDC(CCP)-19/U.

Usachev, L. N. and Bobkov, Yu. G. (1973) - Determination of required accuracy of nuclear data. INDC(CCP)-133/L.

Usachev, L. N. (1974) - Unique definition of nuclear data accuracy. INDC(CCP)-45/L.

internally self-consistent, but does not incorporate the non-linear parts of reactor calculations. The formalism is seen to be useful in discussion of the relationship of constants determined from approximately scaled assemblies in which a large number of nuclear parameters enter identically into any comtemplated calculation. Such similarities may be expected to hold, even for appropriate parameters making non-linear contributions.

The discussion shows, however, that the non-linear effects make any attempt to derive microscopic data from reactor assembly experiments non-competitive for most parameters.

### 4.5 New Reactor Study - Potential of Various Reactor Types for Isotope Production (G. Robinson)

The most important requirement for the new reactor is that it be capable of producing isotopes in sufficient quantity and at a sufficiently high activity to meet future demands. The production of $^{99}Tc^{m}$ by irradiation of molybdenum trioxide is particularly important because of the many applications of this isotope. In addition, inducing a specific activity of the parent isotope, $^{99}Mo$, high enough for export requirements, imposes the most stringent conditions on the reactor flux levels. The desired activity of 6 Ci $g^{-1}$ of $MoO_3$ is four times that currently achieved in HIFAR. The epithermal flux must be high because the epithermal cross section is more substantial than the low thermal cross section of $^{98}Mo$. The requirements are particularly difficult to meet in water moderated reactors which have a high degree of neutron moderation and a compact core. The reactor types included in this study were a $D_2O$ moderated reactor of the HIFAR type and two water moderated reactors, TRIGA and SILOE.

In the consideration of HIFAR type reactors, a direct calculation of HIFAR was made which demonstrated good agreement between calculated Mo activity and that achieved. It would appear that a reactor of this type could be designed to operate at 40 MW and thus give the desired activity. A study of some variations of the reactor core, but retaining HIFAR fuel elements, suggests that by reducing the pitch a reactor operating at only 30 MW would give the required activity.

TRIGA reactors are quite attractive because of their inherent safety obtained by the use of zirconium hydride fuel rods. A study of this reactor type was based on a recent 14 MW design. Calculations of a re-arranged core with a number of high flux irradiation positions gave high thermal fluxes, but an activity of less than 1 Ci $g^{-1}$. TRIGA may therefore be dismissed, as the fuel elements cannot be uprated.

Initial calculations of SILOE were based on the original fuel elements and a core operating at 10 MW. After including a number of central irradiation positions, a larger core operating at 15 MW for the same maximum heat flux as the standard core was required to maintain fuel residence time. For this 15 MW core, the Mo activity was calculated as just over 1 Ci $g^{-1}$. Some information on the uprated SILOE core operating at 35 MW is now available. The fuel elements have been modified to increase the heat transfer surface and special fuel elements, which can include an irradiation sample, have been employed. Samples may thus be included in the core without replacing an entire fuel element. It has been reported that activities of about 2.5 Ci $g^{-1}$ are obtained in the beryllium reflector, which is not the optimum position for Mo irradiation. Activities in the core are to be measured in the near fugure. Several aspects of the reactor physics of the 35 MW SILOE are currently being investigated.

4.6 Other Items

4.6.1 Inverse reaction problem (J. L. Cook, E. Clayton, E, K. Rose)

The study of the determination of nuclear interaction potentials from cross section data has been continued. An error analysis routine has been written which computes the errors in the spatially-group-averaged local potential. Calculations were carried out on the pion-nucleon scattering data and errors obtained for potentials in the seven most important states. One of these states, known as P11, consists of the proton and neutron, and the error analysis revealed that the scattering data could not give detailed information about the inner regions of the nucleon. The errors in the spatially-group-averaged potentials became of order 1000 per cent in the vicinity of the nucleon core, which extends to about 0.2 pion Compton wavelengths.

There are two main classes of potentials in use in nuclear theory; local potentials, which are energy independent, and non-local potentials, which are energy dependent. Theoretical conditions were derived which must be satisfied if a potential is to be local. This condition takes the form of two matrix expressions which must vanish if the potential is to be local. The conditions are very strong ones which the parameters of the reaction matrix must satisfy and give strong correlations between the parameters. Experimental data is being investigated to see how well these conditions are satisfied.

4.6.2 Interactive computer system (G. Trimble, R. Cawley)

Most attention has been given to the development of IBM 360/65 software to enable real time interaction with batch FORTRAN jobs from any AAEC Dataway terminal. An initial version of this real time interactive system has now been written and gives the user the option of either communicating at FORTRAN READ/WRITE level or by use of lower level, single buffer transfers. Additionally, a version of the low level plotting routines has been written which allows graphic data to be sent directly to a display. Both these modules can be used concurrently to give a basic interactive graphics facility. All previously existing high level plotting software can be used with this system. The basic display information is generated in a format that may be used either with a TEKTRONIX display unit, which deciphers the data purely in hardware, or by any 'intelligent' terminal which can translate the information into the appropriate format for its own graphics device.

The implementation of this system has meant that the Physics Division GT-40 computer can now be used to perform real-time interactive graphics with batch central computer jobs. The GT-40 program, HASTE, which handles all communication with the central computer, has been extended to make greater use of the GT-40 display capabilities. This program translates the TEKTRONIX format graphics information into as many as three separate display files which contain the instructions for the display processer. Normally, only one display file is used in which case, the terminal behaves exactly as a TEKTRONIX display unit. The second and third display files may be used to generate dynamic displays or to hold background displays which are turned on and off by the user's IBM 360 program.

One major use of this facility is the examination of the progress of dynamic calculations, such as iteration schemes and the time variation of space/time dependent data. In this case, the scales for the display are held in the first display file and alternate frames of the 'movie' loaded onto files two and three. With the 10 kHz parallel transfer capacity of the Dataway, a speed of about 10 frames per second is achievable for individual frames of 100 vectors. At any time the contents of the display files can be transferred back to the central computer and a hard copy produced on the CALCOMP plotter.

#### 4.6.3 Interactive least squares fitting program (B. E. Clancy)

An interactive program package, SUPERFIT, has been developed for evaluating and plotting a functional form defined by the user and for carrying out least squares fits of the functional form to experimental data values.

In most installations with the necessary computing equipment, sub-programs are available for these tasks, but some sort of control program usually has to be written to control these sub-programs. The control programs, rewritten for each application, usually has the user's functional form coded into it explicitly; if the user's ideas about a suitable functional form change, then the control program has, yet again, to be rewritten.

SUPERFIT provides a general purpose control program which accepts the user's definition of his functional form while the program is executing. The definition is in the form of a sequence of FORTRAN statements and the control program imbeds these in a standard skeleton of coding in such a way as to form a complete program block for evaluating the function at any desired points.

The program operates in an interactive mode and any errors in the user's FORTRAN statements are, when detected, transmitted immediately to the user's terminal so that he may correct them. At any time during a session with the program, the user may elect to change the form of his function. When free from errors, the user's program block is compiled into machine code which is executed, when necessary, by the control program. The actual least squares fitting procedure used is taken from the Harwell subroutine library.

Although the package has been operational for only one month, it has been used with success in a variety of applications. These include:

- fitting a sequence of count rates to the sum of two exponentials,
- fitting a time series of cumulative Norther American oil production figures to the form $y = Q/(1 + A \exp(-Bx))$,
- fitting measured concentrations of $SO_4$ radicals in solution samples to their electrical conductivities by the form $y = (Ax + Bn^2 + Cn^3)/(1 + Dx)$.

### 4.6.4 Applications of unfolding techniques

#### Flux Spectrum Unfolding

(J. L. Cook, H. D. Ferguson)

Interest has long existed in the problem of deducing a neutron flux energy spectrum from the neutron induced activities in a variety of elemental foils, where foils of various elements have been activated by the flux. Knowing the energy format of the cross sections of the foil elements, it is theoretically possible to deduce the flux spectrum from the activation rates. In practice, however, there are difficulties. For a linear least squares analysis, one requires fewer energy group fluxes than foils. Unless one has a very good initial guess of the flux, the group cross sections needed for the calculation will be seriously in error, and the problem becomes ill-conditioned.

One way out of the conditioning problem is to use techniques which have rather more energy groups than foils. Here we require the linear least squares solutions to be constrained by the condition that the $n^{th}$ flux difference be simultaneously minimised. In this way, we find the smoothest solution of all possible solutions. We found that little variation in the solution results, regardless of the difference (0-5th difference) used.

A program was written for the IBM 360/65 which contained three essential testing entities.

1. A library of hypothetical detector cross sections for testing the various theories.

2. A library of actual nuclide group cross sections for doing calculations on specific experiments.

3. A library of hypothetical group flux routines for testing that the group collapsing and solution are satisfactorily conditioned.

The fluxes used were a linear type, a fission spectrum, a full Westcott thermal and epithermal spectrum, as well as a facility for reading in fluxes. The tests of the method with the above were all satisfactory and the hypothetical flux was reproduced in every instance, except where we attempted to reproduce a Westcott spectrum from the library of actual detectors. Here the thermal peak was not reproduced because none of the actual detectors had good resolution in the thermal region, but were designed for fast reactor or fission spectrum types of fluxes. An IAEA test problem listing reaction rates as input, but giving no indication of the flux energy peak shape, was solved and a fission spectrum obtained.

To test the method more thoroughly, we read in step function fluxes and attempted to recalculate them. The solutions obtained, though continuous, gave creditable representations of the discontinuities, though oscillations were present in the region of each discontinuity. These oscillations were almost always within the estimated error in the solutions. If, however, the initial errors were taken to be very small, this situation no longer occurs.

Future work will examine the possibility of establishing a best set of foils for detecting thermal region fluxes, and will compare different overseas methods with our own. As an initial part of this work, four activations carried out in HIFAR by Isotope Division were analysed and a three-group neutron flux calculated. In more sophisticated calculations, however, one should have between 20 and 50 activation detectors to obtain proper details of the flux energy spectrum.

## Spectrum Unfolding - an Alternative Approach

(D. Lang)

In an unfolding problem ambiguities arise if a continuous function is to be determined from a finite set of data values. In activation methods, a set of foils are exposed to the flux. The neutron cross sections are assumed known, and with a known flux, the resultant activity of the foil can be predicted. Given the activities, there are an infinite set of flux spectra capable of generating them.

There is still an unsolved problem of what set of a priori assumptions and consequent restrictions leads to the most sensible description of the flux. A satisfactory set of constraints should be independent of each other. Thus the simplest and most obvious constraint, that the flux should be non-negative at all energies, can lead to difficulties because it is non-linear, and other considerations often depend on a linear formulation of the problem.

Other constraints take the form of minimising some measure of how complicated the spectrum is. It is advantageous to use matrix techniques that can be programmed for eventual computer calculation and which can be related to work in other fields. The complication in structure of a function subject to other constraints can be described by calculating an integral of the square of a quantity that is large in any complicated function. The first choice is the curvature, and hence the second derivative. In consequence, we take the second differences of a function evaluated at a series of equally spread energies. Alternatively, of all functions with the same definite integral between two limits, the one with the least mean square is the one that is a constant between the limits. The integral of the square of any derivative, or of the function itself, can be minimised as a means to cut down the complication in the function.

Minimising the mean square of the flux spectrum then leads to a flux that is a linear combination of the functions describing the cross sections for the various activation reactions. In other resolution studies, the resolution functions which play the same role as the activation cross sections here, are commonly Gaussians or other such simple, smooth functions. A description of a neutron flux as a linear combination of Gaussians is obviously acceptable. Some of the linear combinations of a few multipeaked cross sections are manifestly not credible.

Work is continuing on the production of better constraints and means to incorporate more of the a priori information available.

An interim report on the advantages of the conjugate gradient methods of unfolding noisy data, for reasonable response functions, was presented to the RSIC Seminar Workshop on Unfolding of Radiation Energy Spectra, held at Oak Ridge in April.

Water Chemistry Applications

(D. Lang, E. Clayton)

The proper management of water resources and process waters requires the absolute and relative concentrations of the phytopigments present. These concentrations can be determined from the reflectance spectra when the spectra of individual components are known.

Present techniques of phytopigment analysis involve lengthy chemical separation techniques, followed by transmission spectroscopy of the crudely purified components. Application of mathematical unfolding to reflectance spectroscopy will significantly reduce the time and effort presently spent in chemical analysis.

The aim of this study is to determine the concentration of phytopigments, and hence algal activity in samples taken, for example, from the Georges River or the cooling towers at HIFAR.

Initially, we tried a least squares technique which removed one chlorophyll component from the spectrum and examined the remaining background. This was relatively unsuccessful, as the reflectance spectrum had far more structure than the pure chlorophyll spectrum, and hence its features could not be accounted for solely by the presence of chlorophyll.

An interactive program for the GT-40 has been developed to calculate the maximum concentration by minimising the background. The program allows arbitrary input concentrations and yields evaluation of the spectra directly from plots of the reflectance spectrum and background on the GT-40 screen. As multi-component spectra become available, a more sophisticated unfolding program will be necessary.

4.7 An Australian Energy Data File (K. J. Maher)

In May 1975 a multi-disciplinary group was formed for the purpose of examining energy patterns in Australia. The objective of the group is to investigate the range of conditions under which nuclear reactors could make a worthwhile contribution to Australian energy requirements. The strategy proposed for the long-term investigation is to develop a forecasting model or models of energy usage and resources in Australia. The short-term objective is to investigate the historical and present structure of energy usage.

A preliminary survey by the group of published sources of Australian energy data has revealed a modest volume of statistics, but one that is sufficient to make a computerised compilation worthwhile. The quantity and diversity of data relevant to energy supply and demand forecasting will grow in the future. It is appropriate, therefore, that an energy file should be constructed with generality sufficient to absorb highly disaggregated information. Concurrently, a data management program must be written to allow retrieval and manipulation of a wide range of Australian energy statistics and, at a more aggregated level, population and economic statistics. It is proposed that the data management program will permit interactive access to the file via graphics and printer terminals connected to the Dataway.

The structure of the data file has been defined. It is designed to contain data on consumption, production, imports, exports, state to state flows, reserves, stocks, population, economic indices of production and energy prices. About 50 fuel types can be considered, embracing the wide variety of petroleum products and a range of coals and natural gases. Geographical breakdown can be by states, but finer divisions are possible. End use categories can be broken down to the level of industry and commercial groups used by the Bureau of Census and Statistics. The management program to load, edit and retrieve file data is being written.

5. RUM JUNGLE ENVIRONMENTAL STUDIES (B. Clancy, I. Ritchie)

A weir was constructed in the principal run-off channel of White's overburden heap at the end of the 1975 dry season. The weir is a modified Crump design, developed,in the United Kingdom, to cover rather variable discharge rates similar to those expected in the run-off from White's heap. It has the added advantage that it is self-cleaning. A tipping bucket rain gauge and a conductivity meter were installed at the weir site to measure the conductivity of the water ponded behind the weir. Later in the season, a discrete water sampler was installed. This sampler was capable of taking up to 24 samples of water from the weir pond at preset times after a discharge event had started.

Information on water height in the weir, rainfall and water conductivity, was digitised and recorded on an incremental magnetic tape recording system. Initially, data was recorded every 15 minutes, but this was increased to every 5 minutes later in the wet season. A data processing program has been written that converts the digital information on the tape to water discharge rates, rainfall rates, total discharge volume, total rainfall, etc. Chemical analysis of samples of run-off water has provided a water conductivity $SO_4$ concentration relationship which allows estimates of $SO_4$ concentration and total $SO_4$ loads to be made from the measurements of conductivity.

A total of 66 events were observed from 31st October, 1975, to 26th March, 1976, an event being defined as time when water became ponded behind the weir. Complete records of discharge, rainfall and conductivity have been obtained for 37 events. Discharge rates and partial rainfall rates have been obtained for a further 21 events. Malfunction of both the magnetic tape recorder (battery failures) and the back-up chart recording equipment, cast doubts on the reliability of information from the other 8 events.

Although the results have yet to be fully analysed, a number of important conclusions can be drawn at this stage. The first of these relates to the extreme variability in the nature of the events. Run-off fractions vary between 0.02 per cent and 28 per cent, with as yet no obvious relationship to the total rainfall in the event or the rainfall rate. For example, the event with a run-off fraction of 0.02 per cent lasted for about 4 hours and occurred as the result of 7.4 mm of rain. A few days later, 7.0 mm of rain produced an event, also lasting about 4 hours, but with a run-off fraction of 3.4 per cent. Quite significant rainfalls led, at times, to no discharge over the weir. This emphasises the danger of trying to draw conclusions from one or even a few events.

The second important result is the low value measured for the run-off fraction. The average value for all 58 events, where reliable total discharge and total rainfall data are available, is close to 10 per cent. As the catchment area for the principal run-off channel is about 80 per cent of the surface area of the heap, excluding the walls, it seems reasonable to apply this run-off figure to the heap as a whole. Even allowing for evaporative losses, it appears from the results at this stage that a significant fraction of the rainfall incident on the heap penetrates the body of the heap.

The last important conclusion from the results to hand is that the $SO_4$ levels in the run-off water are low, typically 400 ppm, compared to levels in the spring water, typically 20 000 ppm, flowing from the heap. The result for the $SO_4$ levels in the run-off water is somewhat tentative at this stage, as all the chemical analyses required to confirm the conductivity $SO_4$ relationship are not to hand. However, these data are not expected to alter the estimated levels by more than 20 per cent or so. If it is assumed that the spring water concentrations are typical of all water passing through the body of the heap, then it is clear from the low run-off fraction and the low $SO_4$ levels in the run-off, that the total $SO_4$ burden in the run-off is an insignificant fraction of the total $SO_4$ load associated with water flow from the heap. It is this total $SO_4$ load that appears to be the best indicator of the total amount of oxygen used in whatever oxidation process is taking place in the heap. Results for copper, manganese and zinc concentrations to hand also indicate that run-off water contributes a small fraction of the total heavy metal pollution to the local water system.

Further work has been done on a computer code to solve the water transport equations in unsaturated media. The code calculates water saturation and hydraulic potential levels in a one-dimensional system, following either the introduction of water at the surface (rainfall) or the specification of an initial saturation or hydraulic potential configuration. The code will also estimate if ponding takes place at the surface and the run-off fraction, if any. The code appears to work satisfactorily, but has yet to be checked against reliable experimental data.

Work has also continued on examining means by which oxygen could be supplied to the body of the heap at the rate indicated by the measured $SO_4$ levels. One model is based on the assumption that oxygen supplied by diffusion, through the wet soil to some reaction front in the heap, is the rate limiting process. Estimates of the annual $SO_4$ levels to be expected on the basis of this model and the known physical dimensions of the heap, are the order of those measured and imply that this process is a possible mechanism of oxygen transport.

# 6. PUBLICATIONS

## 6.1 Papers

Allen, B. J., Barrett, R. F., Kenny, M. J. and Bray, K. H. (1976) - Neutron capture mechanism in $^{45}Sc$ and $^{139}La$. Phys. Lett. 61B, 161.

Allen, B. J., Musgrove, A. R., Boldeman, J. W., Kenny, M. J. and Macklin, R. L. (1976) Resonance neutron capture in $^{56}Fe$. Nucl. Phys. (in press).

Barrett, R. F., Allen, B. J., Kenny, M. J. and Musgrove, A. R. (1976) - An investigation of d-wave neutron capture in $^{40}Ca(n,\gamma)$. Phys. Lett. 61B, 441.

Boldeman, J. W., Allen, B. J., Musgrove, A. R., Macklin, R. L. and Winters, R. R. (1976) - Valence neutron capture in $^{88}Sr$. Nucl. Phys. (in press).

Boldeman, J. W., Musgrove, A. R., Allen, B. J., Harvey, J. A. and Macklin, R. L. (1976) - Neutron total and capture cross section of $^{92,94}Zr$. Nucl. Phys. (in press).

Boldeman, J. W., Bertram, W. K. and Walsh, R. L. (1976) - On the question of fine structure in $\bar{\nu}_p$ and $\bar{E}_K$ for $^{233}U$ and $^{235}U$. Nucl. Phys. A265, 337.

Boldeman, J. W. and Walsh, R. L. (1976) - $\bar{\nu}$ for sub-barrier fission in $^{230}Th$. Phys. Lett. 62B, 149.

Clayton, E. and Derrick, G. A. (1976) - A numerical solution of wave equations for real or complex eigenvalues. Aust. J. Phys. (in press).

Cook, J. L., Rose, E. K. and Trimble, G. D. (1976) - Fission product mass yield curves and their energy dependence. Aust. J. Phys. 29, 125.

Kenny, M. J., Joye, A. M. R., Allen, B. J. and Boldeman, J. W. (1976) - Resonance neutron capture in silicon. Nucl. Phys. (in press).

McCulloch, D. B. and Wall, T. (1976) - A method of measuring the neutron absorption cross sections of soil samples for calibration of the neutron moisture meter. Nucl. Instr. & Methods ( in press).

Musgrove, A. R., Allen, B. J., Boldeman, J. W. and Macklin, R. L. (1976) - keV neutron capture cross sections of $^{134}Ba$ and $^{136}Ba$. Nucl. Phys. A256, 173.

Musgrove, A. R., Allen, B. J., Boldeman, J. W. and Macklin, R. L. (1976) - keV neutron resonance capture in barium-137. Aust. J. Phys. 29, 157.

Musgrove, A. R., Allen, B. J., Boldeman, J. W., Chan, D. M. H. and Macklin, R. L. (1976) - Resonant neutron capture in $^{40}Ca$. Nucl. Phys. A509, 170.

Musgrove, A. R., Allen, B. J., Boldeman, J. W., Chan, D. M. H. and Macklin, R. L. (1976) - Odd-even effects in radiative neutron capture by $^{42}Ca$, $^{43}Ca$, $^{44}Ca$. Nucl. Phys. (in press).

Musgrove, A. R., Allen, B. J., Boldeman, J. W. and Macklin, R. L. (1976) - Average neutron resonance parameters and radiative capture cross sections for the isotopes of molybdenum. Nucl. Phys. (in press).

Ritchie, A. I. M. and Rose, A. (1975) - Pulse formation delay times in gas proportional detectors. Nucl. Instr. & Methods, 137, 237.

## 6.2 Reports

Clancy, B. (1976) - SUPERFIT - an interactive program for function evaluation and least squares fitting. AAEC/E report (in press).

Clancy, B. E., Connolly, J. W. and Harrington, B. (1976) - An analysis of power transients observed in SPERT I reactors. Part II: Dependnce of burst parameters on initial temperature and core moderation. AAEC/E383.

Connolly, J. W. and McCulloch, D. B. (1976) - Measurement and calculation of slow power transients in a UTR reactor. AAEC/E report (in press).

Connolly, J. W. and Harrington, B. (1976) - Analysis of power transients in SPERT II core B18/68. AAEC/E report (in press).

Cook, J. L. and Rose, E. K. (1976) - Test of the three-Gaussian assumption for fission product mass yield curves. AAEC/E386.

Donnelly, I. J. (1976) - The accuracy of the diffusion component of removal-diffusion theory. AAEC/E379.

Harries, J. R. (1976) - The circulation of deep water in the Tasman and Coral Seas. AAEC/E390.

Harries, J. R. (1976) - Correlation and flux tilt measurements of coupled-core reactor assemblies. AAEC/E357.

Harrington, B. V. (1976) - AUS module AUSED - an editing program for AUS cross section data pools. AAEC/E389.

Hogg, G. R. and Tendys, J. (1975) - Review of fusion reactor concepts. AAEC/NSTB/PE19.

Knott, R. B. and Harries, J. R. (1976) - The prompt neutron decay constant of the Moata reactor and related coupled-core assemblies. AAEC/E380.

Lang, D. W. (1976) - Resolution unfolding with limits imposed by statistical experimental errors. AAEC/E report (in press).

Maher, K. J., Wilson, D. J., Costello, J. M., Plotnikoff, W. W. and Parkinson, A. (1975) - The nuclear power program and nuclear fuel cycle resources of the COMECON countries. AAEC/NSTB/PE7.

McGregor, B. J., Clifford, C. E., Muckenthaler, F. J. and Mynatt, F. R. (1975) - ORNL TSF pipe chase neutron streaming experiment - Phase 2. ORNL-TM-4283.

McGregor, B. J., Kam, F. B. K., Mynatt, F. R. and Abbott, L. S. (1976) - Calculations of coolant-pipe neutron streaming and secondary coolant activation in the fast flux test facility. ORNL-TM-4446.

Tendys, J. (1976) - Dense plasma focus - a literature review. AAEC/E334.

Trimble, G. D. and Turner, W. J. (1976) - NAIAD - a computer program for the calculation of the steady state and transient behaviour (including LOCA) of compressible two-phase coolant in networks. AAEC/E378.

Wall, T. and Wilson, D. J. (1976) - Neutron flux and background measurements for the proposed uranium analysis rig in HIFAR. AAEC/RP/TN163.

Wilson, D. J. and McGregor, B. (1976) - Thorium utilisation in fission reactors - a summary. AAEC/NSTB/PE16.

### 6.3 Conference Papers

Allen, B. J., Boldeman, J. W., Kenny, M. J., Musgrove, A. R. de L. and Macklin, R. L. (1975) - The neutron capture mechanism: I - capture cross sections. 6th AINSE Nuclear Physics Conf., Melbourne, February.

Bird, J. R. (1976) - Analysis with nuclear reactions. Proc. Aust. Conf. Nuclear Techniques of Analysis, Lucas Heights, May, p. 25.

Bird, J. R., Allen, B. J., Boldeman, J. W., Kenny, M. J. and Musgrove, A. R. de L. (1976) - Resonance neutron capture. Int. Conf. Interactions of Neutrons with Nuclei, Lowell, USA.

Bird, J. R. and Russell, L. H. (1975) - Applications of prompt nuclear analysis techniques to the study of artefacts including Southwest Pacific obsidian. Proc. Symp. Scientific Methods of Study of Ancient Chinese and Southeast Asian Metal Artefacts, National Gallery of Victoria, Melbourne, October 6-10.

Boldeman, J. W. and Walsh, R. L. (1976) - Dynamics of fission. 6th AINSE Nuclear Physics Conf., Melbourne, February.

Boldeman, J. W. and Walsh, R. L. (1976) - Variation of the distributions of mass and kinetic energy as a function of excitation energy in the fission system. Fission induced by low energy neutrons. Études sur la Fission, Aussois, May 24-26.

Campbell, B. L. and Bird, J. R. (1976) - Prompt nuclear analysis - a review and bibliography. Proc. Aust. Conf. Nuclear Techniques of Analysis, Lucas Heights, May 3-6, p. 93.

Clayton, E. (1976) - Neutron detection efficiency calculations for organic detectors. 2nd AIP Congress, Sydney.

Clayton, E. and Cook, J. L. (1976) - Ion application of the inverse reaction problem to pion-nucleon scattering. 2nd AIP Congress, Sydney.

Connolly, J. W. (1976) - A simple model of transient-heat transfer and its application to power excursions in water moderated reactors. 2nd Aust. Conf. Heat and Mass Transfer, Paper RC5.

Ferguson, H. D. and Cook, J. L. (1976) - Determination of neutron flux spectra by constrained linear least squares. Proc. Seminar Workshop on Radiation Energy Spectra Unfolding. ORNL-RISC-60.

Kenny, M. J., Allen, B. J., Bird, J. R., Pe, Hla and Barrett, R. F. (1976) - The neutron capture mechanism: II - capture spectra. 6th AINSE Nuclear Physics Conf., Melbourne, February.

Lang, D. W. (1976) - Analysis of experimental data with effects of random errors. 6th AINSE Nuclear Physics Conf., Melbourne, February.

Lang, D. W. (1976) - Acceptable solutions obtained by unfolding noisy data with a conjugate gradient technique. Proc. Seminar Workshop on Radiation Energy Spectra Unfolding. ORNL-RSIC-60.

McCulloch, D. B. (1976) - Applications of the Moata reactor. Aust. Conf. Nuclear Techniques of Analysis, Lucas Heights, May 3-6.

Owen, D. G., Bird, J. R., Russell, L. H. and Scott, M. D. (1976) - Sodium content of commercial glass. Proc. Aust. Conf. Nuclear Techniques of Analysis, Lucas Heights, May, p. 89.

Conference Papers (cont'd)

Pe, Hla, Allen, B. J., Kenny, M. J. and Bird, J. R. (1976) - Measurement of absolute partial p-wave capture cross sections. Int. Conf. Interactions of Neutrons with Nuclei, Lowell, USA.

Ritchie, A. I. M. and Rose, A. (1976) - Thorium analysis using a pulsed neutron source and delayed neutron counting. Aust. Conf. Nuclear Techniques of Analysis, Lucas Heights, May 3-6.

Scott, M. D., Bird, J. R. and Russell, L. H. (1976) - Solar absorber surfaces. Proc. Aust. Conf. Nuclear Techniques of Analysis, Lucas Heights, May 3-6, p. 45.

Turner, W. J. and Trimble, G. D. (1976) - Calculation of transient two-phase flow. Specialists' Meeting on Transient Two-Phase Flow, Toronto, Canada, August 3-4.

Wall, T. (1975) - Use of the research reactor Moata and associated facilities for the source identification of obsidian artefacts. Conf. Scientific Methods of Research in the Study of Ancient Chinese and Southeast Asian Metal Artefacts, National Gallery of Victoria, Melbourne, October 6-10.

Wall, T. and Bernold, T. X. (1976) - Neutron activation analysis of fluorine. Aust. Conf. Nuclear Techniques of Analysis, Lucas Heights, May 3-6.

Walsh, R. L. and Boldeman, J. W. (1976) - Variation of the distributions of mass and kinetic energy as a function of excitation energy in the fission system. Spontaneous fission of $^{252}Cf$. Études sur la Fission, Aussois, May 24-25.

DISTRIBUTION LIST

AAEC/PR42-P

1. Chairman
2. Deputy Chairman
3. Mr. K. A. Alder, Commissioner
4. Mr. B. J. Callinan, Commissioner
5. Professor H. Messel, Commissioner
6. Program Manager, Nuclear Science and Applications
7. Program Manager, Power and Energy
8. Program Manager, Uranium Fuel Cycle
9. Site Manager
10. Chief, Materials Division
11. Chief, Physics Division
12. Chief, Engineering Research Division
13. Chief, Chemical Technology Division
14. Chief, Instrumentation and Control Division
15. Chief, Isotope Division
16. Head, Applied Mathematics and Computing Section
17. Head, Mechanical Development Section
18. Head, Regulatory and External Relations Branch
19. Secretary
20. Assistant Secretary
21. Director, Information Services
22. Library
23. Director, Nuclear Plant Safety Unit, Mascot
24. Head, Nuclear Studies Group
25. Mascot Library
26. Mr. D. J. Stevens, Director ARL
27. Controller, Site Information Services
28. Controller, Site Administration
29. Controller, Site Operations
30. Controller, Engineering Services
31. Controller Site Planning
32. Manager, Commercial Applications
33. Nuclear Materials Officer
34. ASNT
35. Executive Officer, AINSE

36-38 R.E. Library

39. Washington Office

40-41 London Office

42. Vienna Office
43. Tokyo Office
44. Head, Experimental Reactor Physics Section
45. Head, Neutron Physics Section
46. Head, Theoretical Physics Section
47. Head, Reactor Performance Section
48. Head, Engineering Physics Section
49. Head, Chemical Physics Section
50. Head, Applied Physics Section
51. Head, Health Physics Research Section
52. Head, Radioisotope Services Branch
53. Head, Pharmaceutical & Chemical Products Section
54. Head, Irradiation Research Section
55. Head, Reactor Operations Section

56-96 W. Gemmell for INDC and Bilateral Agreement correspondents

97. B. Allen
98. J. Boldeman
99. J. Connolly
100. J. Cook
101. P. Duerden
102. G. Durance
103. J. Harries
104. G. Hogg
105. M. Kenny

106. D. Lang
107. B. McGregor
108. A. Musgrove
109. J. Pollard
110. M. Rainbow
111. I. Ritchie
112. J. Tendys
113. W. Turner
114-144 J. R. Bird (for special distribution)
145. D. Byers (University of Canterbury, N.Z.)
146. V. Deniz (BARC, India)
147. S. Kapoor (BARC, India)
148. N. Veeraraghavan (BARC, India)
149. G. K. Mehta (Indian Institute of Technology)
150. S. Supadi (BATAN, Bandung)
151. I. Supki (BATAN, Bandung)
152. G. Tyror (AEEW, UK)
153. J. Askew (AEEW, UK)
154-174 Bilateral Agreements (UKAEA 5, US ERDA 11, AECL 5) via H.O.
175-185 Spares